CHAPTER 3

Continuous monitoring with *in situ* sensors

Daniel Dzurisin

The previous chapter described several ways to measure volcano deformation by making repeated network surveys. Frequent surveys of a well-designed network can serve to characterize the deformation field in space and time, albeit not completely nor continuously, thereby helping to constrain source models and anticipate future activity. However, this approach has two serious shortcomings during a crisis: (1) it repeatedly places survey personnel near a hazardous volcano, potentially in harm's way; and (2) repeated surveys cannot always keep pace with a rapidly evolving crisis, especially at night or during bad weather. Therefore, it is desirable to supplement periodic geodetic surveys with carefully sited continuous sensors that provide a steady stream of data in real time for analysis. Continuous monitoring also is important during non-crisis periods, because it can: (1) detect changes in the deformation pattern sooner than repeated surveys; (2) provide a dense time series of data as context for evaluating subtle changes in the pattern or rate of deformation; and (3) reduce the need for recurring field operations.

A disadvantage of *in situ* monitoring is that each sensor responds to its immediate surroundings, which may or may not represent the deformation field as a whole. If care is taken to couple sensors adequately to the ground and to insulate them from near-surface environmental effects, this shortcoming can be overcome in most cases. However, success is never guaranteed even with the most careful installations, so some type of redundancy is always desirable. For example, multiple sensors or sensor types might be installed near each other as a consistency check, or surveys might be conducted periodically near the stations to assess the reliability and fidelity of the continuous data. To optimize the design of a continuous sensor network for a particular situation, station locations should be chosen based on the results of repeated surveys or, in the absence of measured deformation, based on numerical models of the deformation field for plausible source types (Chapter 8).

This chapter describes five types of *in situ* deformation sensors: tiltmeters, strainmeters, continuous Global Positioning System (GPS) stations, gravimeters, and differential lake gauges, and discusses their use at selected volcanoes. Also included is a brief discussion of seismometers, for three reasons: (1) seismometers are used more than any other type of *in situ* sensor to monitor volcanoes; (2) the widespread use of broadband seismometers, borehole strainmeters, and continuous GPS instruments to record such phenomena as very long period (VLP) earthquakes and 'slow' earthquakes (e.g., Hill *et al.*, 2002b; Dragert *et al.*, 2001; Section 4.8.5) has blurred the traditional boundary between seismology and geodesy; and (3) to save the reader interested in a brief introduction to seismological concepts the task of looking elsewhere. Those seeking a more detailed treatment of modern volcano seismology might want to consult reviews of the subject by Chouet (1996b, 2003) and McNutt (1996, 2000a,b). Additional information on the use of GPS receivers and strainmeters to monitor volcano deformation is provided in Chapters 4 and 9, respectively.

3.1 SEISMOMETERS

No book about volcano monitoring would be complete without at least a brief discussion of seismometers and seismological principles. Volcano seismology and volcano geodesy have been closely linked throughout the modern era of geophysical instrumentation, which spans more than a century.

D. Dzurisin, *Volcano Deformation*

The linkage arose partly because early seismometers were sensitive to ground tilt (Section 1.4.1), modern tiltmeters and strainmeters are capable of recording long-period (LP) and VLP earthquakes, and broad-band seismometers respond to ground motions with periods as long as ~50 s. In recent years the two disciplines have become increasingly intertwined as new discoveries reveal the full spectrum of Earth motions, including: (1) bradyseisms[1] with periods of months to decades, (2) slow earthquakes (days to weeks), (3) ultra long-, very long-, and long-period earthquakes (seconds to minutes), and (4) predominantly short-period earthquakes produced by brittle rock failure along faults (<0.1 to 1 second). The following treatment is basic and by no means complete, but it should suffice for most readers in lieu of consulting one or more of the review papers mentioned in the preceding paragraph.

3.1.1 A brief history of seismology

Aristotle (ca. 330 BCE) attributed earthquakes to winds blowing in underground caverns, and Chinese philosophers at about the same time suggested that ground shaking was caused by the blocking of a subtle essence (the *qi*). Chinese mathematician and philosopher Zhang Heng (or Chang Hêng) is credited with inventing the first seismoscope, which is reported to have detected a four-hundred-mile distant earthquake that was not felt at the location of the instrument, in 132 CE (Dewey and Byerly, 1969; Needham, 1959). An early association between earthquakes and volcanoes developed during the scientific revolution in Europe between roughly 1500 and 1700. Familiarity with gunpowder led various writers to attribute both phenomena to explosions in the Earth resulting from combustion of pyrites or a reaction of iron with sulfur (Agnew, 2002).

The first recognition that ground shaking was caused by waves in the Earth propagating from a specific location came shortly after the destructive Lisbon earthquake of 1755, but a revolutionary 'new seismology' did not emerge for another century. The Meiji restoration of 1868 in Japan led to the establishment of modern science in a very seismic region, facilitated by foreign experts including John Milne, James A. Ewing, and Thomas Gray, who worked at prestigious Japanese universities at the invitation of the national government. Ewing and Gray used a horizontal pendulum[2] to produce the first good instrumental records of ground shaking, while Milne pioneered the field of global seismology. Agnew (2002) describes a 'classical' period in seismology that followed from 1920 to 1960, when ideas about wave propagation were refined and improved but there were no substantial technical advances. Interestingly, this period began shortly after Dr. Thomas A. Jaggar founded the Hawaiian Volcano Observatory (HVO) in 1912, and it ended shortly after Professor Kiyoo Mogi published his classic paper on volcano deformation (Mogi, 1958). Most volcanologists I know do not shy away from the fact that seismology often leads volcanology, especially in the theoretical arena. We tend to be pragmatists who welcome any source of insight into how real-world volcanoes work.

The modern era in seismology can be pegged to the emergence of plate tectonics theory starting in

[1] 'Bradyseism' refers to slow uplift or subsidence of the ground surface in response to inflation or deflation of a magma reservoir, or to pressurization or depressurization of a hydrothermal system. The best known example is the remarkable motion of the Phlegraean Fields caldera near Naples, Italy, which has persisted since Roman times.

[2] The horizontal pendulum was first described in 1832 by priest and scholar Lawrence (Lorenz) Hengler, who noted its utility as an astronomical instrument capable of measuring slight deviations from vertical. Zöllner (1869) was the first to suggest its use as a seismometer, and on 17 April 1889, von Rebeur-Paschwitz (1889) obtained one of the first known recordings of a distant earthquake using such a device. The earthquake had been felt in Japan about an hour before its surface waves were recorded in Germany. To achieve its remarkable sensitivity, the horizontal pendulum takes advantage of some basic physics. The more familiar vertical pendulum, consisting of a mass suspended on a string, oscillates with period $T = 2\pi\sqrt{L/g}$, where L is the length of the pendulum and g is acceleration due to gravity. For a rigid pendulum swinging in an inclined plane, the oscillation period is given by: $T = 2\pi\sqrt{L/g\sin\theta}$, where θ is the inclination from horizontal. Note that, as L approaches infinity or $g\sin\theta$ approaches zero, T tends toward infinity. Increasing L indefinitely has practical limitations, but dialing down the effect of gravity by decreasing θ turns out to be both easy and elegant. For an intuitive example, consider a gate swinging on a vertical hinge-post. If the post is exactly vertical, the gate swings freely through every position (ignoring friction). If the post is inclined slightly, the gate assumes an equilibrium position that is very sensitive to the orientation of the post. Once the gate is set into motion, it oscillates about the equilibrium position for a long time (θ is small, so T is large). Small changes in the orientation of the post produce large changes in the equilibrium position. In a horizontal-pendulum seismograph, a mass attached to one end of a rigid beam is free to oscillate in a horizontal plane about a vertical hinge near the other end of the beam. This arrangement is extremely sensitive to horizontal accelerations, including those caused by the passage of seismic waves. Add a means to record the swings of the mass at the pendulum's tip, and you have a functional seismograph.

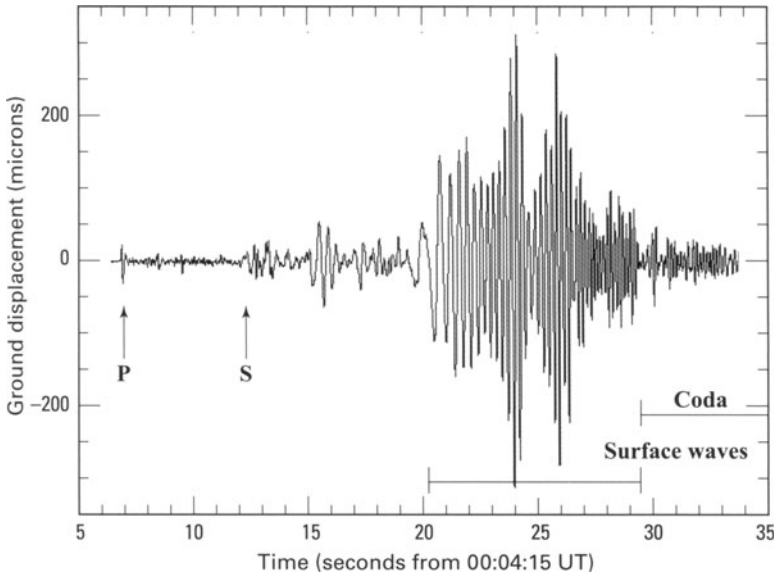

Figure 3.1. Seismogram showing vertical surface motion recorded at Kevo, Finland, beginning 500 seconds (8.3 minutes) after the start of the 17 October 1989, M_s 7.1 (M_w 6.9) Loma Prieta, California, earthquake near San Francisco. The distance from the epicenter to the seismometer is 71° (~7,880 km). Arrows indicate first arrivals of the P- and S-waves (body waves); bars show duration of surface waves and first ~5 s of the trailing coda. See text for discussion.

1960 (e.g., Vine and Matthews, 1963; Vine, 1966). Increasingly precise locations for sea-floor earthquakes placed most of them along mid-ocean ridges, focal-mechanism studies showed that oceanic fracture zones behave as transform faults connecting segments of the spreading ridge, and seismologists recognized that the distribution of many deep earthquakes, which theretofore had been enigmatic, was organized along subduction zones. As a historical note, Dr. Robert W. Decker and colleagues at HVO made the first electronic distance meter (EDM) measurements at Kīlauea and Mauna Loa Volcanoes in the 1960s, amidst the early excitement over plate tectonics. At the time I was a teenager fascinated by Solar System exploration, including the quest to land astronauts on the Moon. Another decade passed before I realized that Earth was the only planet I would ever visit, and volcanoes were among the most interesting things on Earth.

3.1.2 An introduction to seismic waves and earthquake types

Seismic waves are of two types: short-period (high-frequency) body waves that travel within the Earth and long-period (low-frequency) surface waves that travel along its surface. Body waves include longitudinal P-waves and transverse S-waves. P-waves travel faster than S-waves and arrive earlier; hence the designations P- (primary) and S- (secondary). P-waves involve compressional particle motion in the direction of wave propagation; S-waves involve shear (sideways) motion. P-waves propagate through liquids, including magma and partial melt, but S-waves disappear or are greatly attenuated.[3]

There are also two types of surface waves, Love waves and Rayleigh waves.[4] Surface waves travel slower than body waves but they attenuate less with distance. Surface waves from great earthquakes travel completely around the globe many times. They are responsible for most of the ground shaking produced by distant large earthquakes. Great earthquakes also excite free oscillations of the entire Earth, akin to the ringing of a giant bell, which can persist for days.

[3] Because liquids are largely incompressible and do not support shear stress, P-waves propagate through them but S-waves do not. Magma and hydrothermal fluids are compressible to varying degrees owing to the presence of gas in bubbles. As a result, S-waves and, to a lesser degree, P-waves are attenuated in magmatic and hydrothermal environments. Seismic tomography is a technique used to delineate the 3-D shapes of magma bodies and hydrothermal systems by mapping out S-wave attenuation along intersecting ray paths from a large number of earthquake sources to a dense array of seismometers.

[4] Love waves and Rayleigh waves travel along the surface of the solid Earth. They are distinct from T-waves, which are short-period (≤1 s) acoustic waves that travel in the ocean at the speed of sound in water. A 'T-phase' is occasionally identified in the records of earthquakes in which a large part of the path from epicenter to station is across the deep ocean.

The first noticeable indication of an earthquake is often a sharp 'thud' signaling the arrival of the fast-moving compressional P-wave. This is followed by the S-wave and then the more gentle 'ground roll' caused by surface waves. P-waves, because they are the first to arrive, are used to locate earthquakes based on their differential travel times to an array of seismometers at different azimuths (directions) and distances from the earthquake's focus. S-waves and surface waves contribute to the concluding train of seismic waves, called the coda, which follows the primary wave (Figure 3.1). Codas from great earthquakes continue for hours while the slowly attenuating surface waves repeatedly circumnavigate the globe.

The frequencies of seismic waves range from as high as the audible range (greater than 20 Hz) to as low as the free oscillations of the Earth, with a longest period of 54 minutes (corresponding to a frequency of 0.0003 Hz). The amplitude range of seismic waves is also large. Measurable ground displacements from small to moderate earthquakes range from about 10^{-10} to 10^{-1} meters (0.1 nanometer (nm) to 1 decimeter). For comparison, the smallest displacement measured for geodetic purposes, to my knowledge, is ~1 nm – the resolution of a differential transformer in a Sacks–Evertson borehole strainmeter (Section 9.1).[5] In the greatest earthquakes, the amplitude of the predominant P-waves can be several centimeters at periods of 2 to 5 s. Very close to the epicenters of great earthquakes, peak ground accelerations sometimes exceed that of gravity at high frequencies, and ground displacements can reach 1 m at low frequencies.

Reports of earthquake sounds are common, even though the dominant frequency of seismic waves is well below the audible range for most humans.[6] Most reports of a roar or train-like sound associated with moderate-to-large earthquakes undoubtedly refer to non-seismic noise sources such as objects crashing to the ground, breaking, or jostling together under the influence of seismic waves, rather than any sound generated by the waves themselves. Nonetheless, there are many credible reports of a boom or thud being heard close to the epicenter of small (M 2–4) earthquakes. I have heard such a noise dozens of times during swarms of earthquakes at Kīlauea and Mount St. Helens Volcanoes. Often the sound is followed almost immediately by perceptible ground shaking, but in some cases even shocks too small to be felt can be heard. Apparently, high-frequency ground vibrations couple to the atmosphere well enough to produce audible pressure pulses, at least within a few kilometers of the source. The sound of the Earth quivering like a drumhead in response to the beat of an earthquake is at once ominous and beguiling – a primal resonance that commands attention and instills a sense of vulnerability in even the most intrepid volcano watcher.

Any classification scheme for something as complicated and diverse as seismic events beneath volcanoes is fated to be revised as new information becomes available or new theories emerge to describe the causative processes. Nonetheless, a simple proposal by Japanese seismologist and volcanologist Takeshi Minakami (1960, 1961) has enjoyed considerable longevity. Minakami divided volcanic earthquakes into two types based on their signatures on seismograms and on their source depths. A-type earthquakes have a clear P-wave and S-wave and generally occur at depths of 1–10 km beneath a volcano. They are indistinguishable from normal shallow tectonic earthquakes. B-type earthquakes have emergent P-wave signatures on seismograms (i.e., gradual onsets), no distinct S-wave, and low-frequency content relative to tectonic earthquakes of the same magnitude. Minakami (1961) attributed the character of B-type earthquakes to an extremely shallow focal depth (<1 km). Poorly consolidated near-surface materials at most volcanoes attenuate high frequencies in P-waves and transmit S-waves very poorly, which could account for the characteristic signature of B-type events.

Recently the contrast between A-type and B-type earthquakes has been attributed to different source processes rather than to shallow path effects (e.g., Chouet, 1988, 1992, 1996a). Currently, A-type events are more often called volcano–tectonic (VT) or high-frequency (HF), and B-type events are called long-period (LP) or low-frequency (LF). VT earthquakes are attributed to brittle

[5] The wavelengths of ultraviolet radiation and visible light are short enough to be measured in nanometers. Most of the UV radiation that reaches the Earth from the Sun has wavelengths 100–400 nm, and visible light has wavelengths of 400–700 nm.

[6] Numerous claims of pets or other animals acting strangely before a damaging earthquake remain unsubstantiated or unexplained, as do frequent earthquake 'predictions' by non-scientists based on a sense of impending calamity or some other indicator. Science is always open to discoveries that revise current understanding of the natural world, but for now predicting an earthquake before the arrival of the P-wave is mostly outside the scientific mainstream. Prediction is one arena in which volcanology leads seismology: At a time when successful eruption predictions are becoming more common, earthquake prediction remains an elusive research goal.

rock failure and, except for their occurrence near a volcano, are indistinguishable from normal tectonic earthquakes that occur elsewhere. LP events are attributed to resonance in a fluid-driven crack under choked-flow conditions (Chouet, 1988, 1996a; Chouet *et al.*, 1994), fluid pressurization processes such as bubble formation and collapse, and oscillation of a fluid-filled cavity (McNutt, 2000a,b). An alternative explanation has been proposed for deep LP (DLP) events that heralded the 1991 VEI[7] 5-6 eruption of Mount Pinatubo, Philippines, and which occur sporadically in the lower crust beneath some volcanoes in the Aleutian arc, for example. White (1996) and Power *et al.* (2004) attribute DLP earthquakes to injections of mixed phase (liquid + gas) basaltic fluids upward through cracks from the upper mantle or mid-to-lower crust into the roots of volcanoes.

Some volcanic earthquakes 'straddle the fence' between VT and LP types (i.e., they share attributes of both). They are called hybrid events and are thought to represent a combination of processes, such as an earthquake occurring near a fluid-filled crack and setting it into oscillation (McNutt, 2000a,b).

Another type of volcanic seismicity is tremor, which produces a continuous signal on seismographs with a duration of minutes to days or longer. The dominant frequencies of volcanic tremor are 1–5 Hz; 2–3 Hz is most common. This is similar to the frequency content of LP earthquakes, which leads many investigators to conclude that tremor is a series of closely spaced LP earthquakes. Two special types of volcanic tremor are harmonic tremor and spasmodic tremor. As the name implies, harmonic tremor consists primarily of a single-frequency sinusoid with smoothly varying amplitude; in some cases, a fundamental frequency is accompanied by its overtones (i.e., 'harmonics').[8] Spasmodic tremor is higher frequency, pulsating, and irregular in amplitude.

The origin of tremor has received considerable attention from volcano seismologists for decades. The observation that Hawai'ian eruptions are always accompanied by harmonic tremor suggests that magma flow through shallow conduits is involved in the source mechanism. The harmonic nature of some tremor can be modeled as resonance in a fluid-filled crack, akin to one of the mechanisms invoked to explain LP earthquakes (Chouet, 1988, 1992). Similarly, spasmodic tremor can be interpreted as unsteady flow in a volcanic conduit under choked-flow conditions. Although different mechanisms might operate in different situations, it seems appropriate to think of most tremor as one or more LP earthquakes, persisting either because the same fluid-filled source is repeatedly excited or because many similar sources are active in a small volume.

For additional discussion of types of volcanic earthquakes, terminology, and inferred source mechanisms, the reader is referred to, for example, Chouet (1996a, 2003) and McNutt (1996, 2000a,b).

3.1.3 Basic principles of seismometers

Although the modeling and interpretation of seismic waves is mathematically complex, seismic instrumentation is mechanically simple by comparison (e.g., Telford *et al.*, 1990, pp. 136–282). Geophones consist of four basic elements: (1) a frame securely affixed to the Earth, ideally embedded in solid bedrock deep enough to substantially attenuate surface noise; (2) an inertial mass suspended in the frame, called a proof mass, with a steady-state reference position established by springs (horizontal pendulum), gravity (vertical pendulum), or electrical forces (broadband seismometer); (3) a damper system to prevent long term resonant oscillations; and (4) a means of recording the motion of the mass relative to the frame. Passing seismic waves move the frame, while the mass tends to remain in a fixed position due to its inertia. The relative motion is sensed and recorded to produce a seismogram. Early seismometers used mechanical linkages to amplify the motion of the suspended mass. Modern instruments use electronic amplification of signals generated by position or motion sensors (Telford *et al.*, 1990, pp. 195–197).

The Mark Products L4C geophone is widely used for earthquake and volcano studies, and its design illustrates the basic elements of modern, short-

[7] Volcanic Explosivity Index (VEI) a measure of the size of volcanic eruptions akin to the Richter magnitude scale for earthquakes. The VEI is a 0-to-8 index of increasing explosivity, each interval representing an increase of about a factor of ten. It combines total volume of explosive products, eruptive cloud height, descriptive terms, and other measures (Newhall and Self, 1982).

[8] A 'harmonic' (noun) is a mode of vibration whose frequency is an integral multiple of a fundamental or base frequency; a series of oscillations is referred to as 'harmonic' (adjective) when each oscillation has a frequency that is an integral multiple of the fundamental frequency (i.e., each oscillation is a 'harmonic' of the fundamental frequency). Thus, the frequency content of harmonic tremor includes a fundamental frequency and its harmonics. If you're confused, complain to a seismologist.

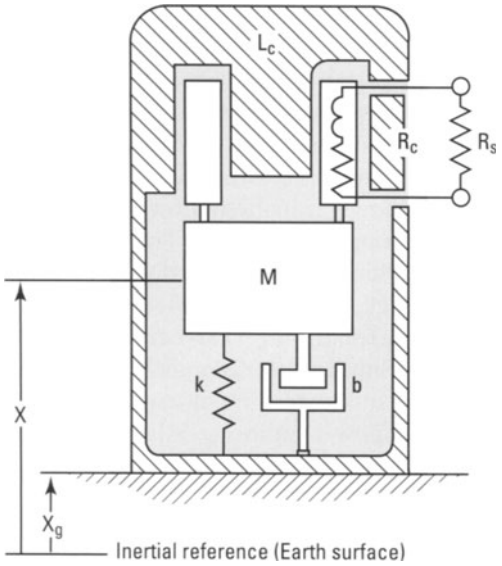

Figure 3.2. Mark Products vertical L4C geophone, from Bowden (2003). A proof mass M (kg) is suspended by a spring with stiffness k ($n \times m^{-1}$) and mechanically damped by dashpot b ($n \times m^{-1} \times s^{-1}$). The motion-sensing coil is mounted above the proof mass and is represented by inductance L_c in series with coil resistance R_c. See text for details.

period seismic sensors (Figure 3.2). The following description of the L4C closely follows Bowden (2003, pp. 1–2). The sensor produces a voltage proportional to the velocity difference $(dx/dt - dx_g/dt)$ between its proof mass M and its housing. Voltage is generated in a pickup coil wound on the proof mass when a permanent magnet attached to the housing moves past the coil. The suspension system consists of a 1 kg mass suspended on soft springs with resonant frequency around 1 Hz. The system acts as a damped mechanical oscillator electromagnetically coupled to the output by the moving field of the permanent magnet. For ground motions at frequencies above mechanical resonance, the output signal follows the ground velocity, dx_g/dt. For frequencies below resonance, voltage falls off as proof mass motion starts to follow ground motion.

Modern seismometers come in two types, analog and digital, and three main varieties: short-period, long-period, and broadband. Most applications use either a single-component sensor oriented such that it responds to vertical motions, or a three-component sensor that responds along the vertical axis and two orthogonal horizontal axes. Analog seismometers are very sensitive to ground motion but they have a limited dynamic range (i.e., they 'clip' or go off-scale for most earthquakes large enough to be felt). The heart of a broadband seismometer is a small mass confined in space by electrical forces. As the Earth moves, sophisticated electronics attempt to hold the mass steady through a feedback circuit. The force necessary to achieve this is proportional to ground acceleration ($F = ma$), which can be integrated to yield velocity and then output to a recording or telemetry system.

Digital broadband seismometers are more expensive, require more power, and are more difficult to deploy and maintain in the field than analog short-period instruments, which were the mainstay of volcano monitoring for several decades. However, the ability to record a broad range of frequencies, from about 0.02 Hz to 50 Hz (corresponding to periods of 50 s to 0.02 s), while staying on-scale through a wide range in earthquake induced ground motions, has made digital broadband seismometers increasingly popular among volcano seismologists during the past decade (e.g., McNutt, 1996). With records from an array of three-component, digital broadband instruments, seismologists can ogle, compare, and model the complete codas of thousands of earthquakes. Better them than me, but I am not a seismologist (a fact made clear to me on numerous occasions).

3.1.4 Current research topics in volcano seismology

Volcano seismology aims to understand the structure of magmatic and hydrothermal systems, the source mechanisms of volcanic seismicity, and the spatial and temporal patterns of magma transport through the crust. An overarching goal is to characterize magmatic systems well enough to enable the development of quantitative models capable of accounting for observed seismicity and of predicting future developments, including eruptions. Such an ambitious agenda requires that the scope of cutting-edge research be both broad and rapidly evolving. Consequently, rather than trying to paint a complete picture of the current state-of-the-art in volcano seismology, I have included just a snapshot of a few particularly vibrant topics in the field. The interested reader will find considerably more detail in the review article by Chouet (2003) and references therein.

Although determination of the seismic velocity structure of the Earth is a time-honored undertaking for seismologists, new instrumentation and approaches keep the work fresh and productive. For example, the 3-D velocity structure of a volcanic edifice can be imaged in unprecedented detail using

high-resolution travel-time tomography. The technique uses crisscrossing ray paths from a large number of local earthquakes to a dense array of seismic stations to map local departures from an initial velocity model through comparison of predicted and observed arrival times. The result is an improved image of the 3-D velocity structure, typically with a spatial resolution of 1 km or better (Chouet, 2003).

Dawson *et al.* (1999) used tomographic inversion[9] of 4,695 P-wave and 3,195 S-wave arrivals from 206 earthquakes during a 20-day period in 1996 to derive high-resolution (0.5 km) 3-D P-wave velocity and V_P/V_S models of the Kīlauea Caldera region, Hawai'i.[10] The models delineate a zone of anomalously low P-wave velocities at depths of 1–4 km centered beneath the southeastern rim of the caldera, including two smaller zones of high V_P/V_S beneath the southern portion of the caldera and the upper East Rift Zone. The latter are interpreted as magma storage zones, consistent with many other studies that point to reservoirs in those areas.

The source mechanism of most VT earthquakes (brittle failure of rock) is well understood owing to their similarity to normal tectonic earthquakes, but the mechanisms of LP volcanic earthquakes and volcanic tremor remain fertile topics for research. The pioneering work by Aki *et al.* (1977), who interpreted volcanic tremor using fluid-driven crack models, inspired additional breakthroughs by Chouet (1981, 1985, 1986, 1988, 1992, 1996a) and others during the ensuing two decades. The resulting theoretical framework, which draws heavily upon the dynamics of multiphase fluids, serves as a point of departure for most contemporary analyses.

One particularly promising facet of current research involves the use of dense, small-aperture arrays of short-period seismometers to delineate the source regions of LP earthquakes and tremor. As noted by Chouet (2003), this type of seismicity cannot be located by conventional means because the signals' first arrivals on seismograms are emergent, not impulsive (i.e., gradual, not sudden). To locate a seismic event, the relative timing of its first arrival at several stations must be known precisely (seismic waves travel at speeds of several km s^{-1}, so small timing errors have a big effect on the accuracy of the hypocenter location). This generally is not possible for emergent signals, whose first arrivals are obscured by unavoidable environmental and system noise (the slightly wavering background signal on an otherwise quiet seismogram). To circumvent this problem, Chouet and his colleagues deploy arrays of closely spaced seismometers around a source of LP events or tremor to act as seismic wave antennas.

One such array at Kīlauea Volcano, Hawai'i, consisted of 41 three-component sensors arranged in a semicircular spoked pattern with 50-m spacing along the spokes and 20° angular spacing between spokes. Each of several antennas (three in this case) provides a vector, called the slowness vector,[11] which represents the propagation direction and apparent velocity of seismic wave fronts across the array. The slowness vector data are combined with a model of the seismic velocity structure and inverted to produce a 3-D map of the source volume (Almendros *et al.*, 2001a). Results for Kīlauea obtained during a swarm of LP events and tremor in February 1997 are very similar for both event types and point to a hydrothermal origin (Almendros *et al.*, 2001b; Chouet, 2003). Those authors suggest that the swarm was a hydrothermal response to enhanced degassing associated with increased magma transport in Kīlauea's deeper magma conduit system.

[9] There are two general approaches to modeling geodetic and geophysical data, called *forward* and *inverse* methods (Chapter 8). Forward models use physical principles and known (or assumed) material properties to calculate a theoretical system response. For example, the surface-displacement field caused by a given pressure change in a Mogi-type source embedded at a given location and depth in a semi-infinite half-space with given elastic properties can be calculated using a forward model. An inverse model, on the other hand, starts with a generalized forward model and uses observations (data) with their associated uncertainties, plus known (or assumed) constraints called boundary conditions, to determine the best-fitting parameters for the model. This is accomplished by minimizing some model-to-data misfit criterion. For example, leveling or GPS data can be 'inverted' to determine the parameters of a Mogi source, including the optimal pressure change, location, and depth, that best fits the data in a least-squares sense. Inversion problems can be either linear or nonlinear, depending on the physics involved. Nonlinear inversions are non-unique, and require stronger constraints (e.g., more and better data, or independent knowledge of the system) to achieve a satisfactory result.

[10] V_P/V_S is the ratio of P-wave velocity to S-wave velocity. S-waves are more attenuated than P-waves by the presence of fractures, hydrothermal fluids, or partial melt, so the combination of relatively low P-wave velocity and high V_P/V_S is an indicator of pervasively fractured or fluid-rich zones within a volcanic edifice.

[11] Slowness is defined as the inverse of velocity for seismic waves; a large slowness corresponds to a low velocity. Most seismic tomography methods involve subdividing the medium into blocks and solving for slowness perturbations that cause predicted arrival times to match observed arrival times better than an initial model.

Another fruitful line of investigation uses moment tensor[12] inversion of VLP data (events with periods ranging from tens of seconds to a few minutes) recorded by broadband seismometers to infer magma conduit geometry and mass transport phenomena (Chouet, 2003). For example, Ohminato *et al.* (1998) analyzed broadband data acquired during a 4.5-hour period of rapid summit inflation and increasing seismic activity in the Kīlauea summit region on 1 February 1996. When the data are low-pass filtered and converted to displacement, they reveal a repetitive sawtooth signal with a rise time of 2–3 minutes and a drop time of 5–10 s.[13] What mechanism could account for mini inflation–deflation cycles with periods of just 2–3 minutes?

Ohminato *et al.* (1998) showed that the data are consistent with oscillations of a sub-horizontal crack or sill-like structure located about 1 km beneath the floor of Kīlauea Caldera. The volume change estimated from seismic moments of individual VLP events is $1\text{–}4 \times 10^3\ m^3$, and integration over the duration of VLP activity yields a net volume budget on the order of $5 \times 10^5\ m^3$. To explain the observations, the authors proposed a conceptual model of separated gas–liquid flow through a converging–diverging nozzle under choked conditions (Figure 3.3). During an inflation phase, magmatic gas accumulates upstream of the nozzle, building excess pressure and deforming the crack as a result. The gas slug is essentially stationary and the Mach number of the gas is $M_g \ll 1$. This phase coincides with the upgoing ramp in the sawtooth displacement signals. Eventually, pressure builds to the point that some of the gas is able to displace magmatic liquid and escape through the constriction in the nozzle. The gas flow is choked ($M_g = 1$) in the nozzle and is supersonic ($M_g > 1$) immediately downstream of the nozzle. This phase corresponds to the rapid downdrop segment in the sawtooth displacement signals. Gas escape quickly lowers the pressure upstream of the nozzle, which again fills with liquid, thereby halting the gas flow and starting the cycle anew. In this fashion, 500,000 m^3 of magma apparently chugged its way through a constriction in Kīlauea's shallow magma plumbing system during a 4.5-hour period, leaving behind as evidence some very long-period seismic fingerprints. That is an impressive story to extract from seemingly chaotic wiggles on broadband seismograms!

There are many other exciting research topics in contemporary volcano seismology, including precise relative relocation of swarm earthquakes to better delineate fault planes and other seismically active structures (e.g., Rubin *et al.*, 1998; Prejean *et al.*, 2002; Hill *et al.*, 2003; Got *et al.*, 2002; Got and Okubo, 2003; Battaglia *et al.*, 2003),[14] source mechanisms and implications of earthquake multiplets (e.g., Got *et al.*, 1994; Ramos *et al.*, 1996; Poupinet *et al.*, 1996; Got and Coutant, 1997),[15] spectral analysis of LP events to determine acoustic properties of magmatic and hydrothermal fluids (Kumagai and Chouet, 2000), and experimental modeling of the source dynamics of tremor (Lane *et al.*, 2001). Readers wanting to learn more about these topics might want to consult the original literature or a recent review article (e.g., Chouet, 2003).

Hopefully this section has conveyed a sense of the great breadth and diversity of contemporary research topics in volcano seismology. Now let us turn our attention back to geodesy and some additional tools of the ground deformation monitoring trade.

[12] The earthquake (or seismic) moment tensor is a symmetric, second-order (3 × 3) tensor that describes the nature of a fault's motion in terms of the amount of seismic moment release. Its components are 9 force couples, M_{ab}, where a and b correspond to the x, y, z axes, and $M_{ab} = M_{ba}$. Each force couple consists of two forces of magnitude f, separated by distance d, acting together in opposite directions; the magnitude of each component is the scalar moment, $f \times d$. Moment tensors corresponding to slip on a fault plane have a zero trace ($M_{xx} + M_{yy} + M_{zz} = 0$); a nonzero trace implies a volume change. The latter source type, sometimes referred to as a 'non-double--couple' source, is of particular interest in volcanology. Non-double--couple sources include explosions, implosions, and fluid injections into expanding cracks. For more information, the interested reader is referred to a seismology textbook such as Stein and Wysession (2003) or Aki and Richards (1980).

[13] Low-pass filtering the broadband signals removes higher frequency information that is superfluous for the analysis described here, but which can be analyzed separately to shed light on other volcanic processes.

[14] Relative relocation algorithms take advantage of the fact that errors in *absolute* hypocenter locations are largely attributable to sources, such as an imperfect seismic-velocity model, that affect tightly clustered events more or less equally (i.e., the errors are common-mode). The effect of common-mode errors can be reduced to the extent that hypocentral errors shrink by one to two orders of magnitude, revealing such structures as active fault planes and magma pathways (e.g., Prejean *et al.*, 2002).

[15] 'Earthquake multiplets' refers to a group of seismic events, usually occurring in a swarm, with very similar signatures (codas) on seismograms. In some cases, multiplet codas are virtually identical -- to the extent that the events appear to be clones of one another. At least some multiplets are thought to indicate repetitive, non-destructive excitation of the same source (e.g., opening and closing of a fluid-filled crack, bubble oscillation, or stick--slip motion across a resilient seismic patch on an otherwise freely slipping fault surface).

3.2 TILTMETERS

A review paper on the uses of strainmeters and tiltmeters published in 1986 began with a rather gloomy assessment: '*Despite steady effort over the last century, continuously recording tiltmeters and strainmeters have not yet been successful except for earth tide measurements*' (Agnew, 1986, p. 579). Since then, the situation has brightened considerably. The use of tiltmeters and strainmeters to monitor volcano deformation has become increasingly common, and there have been several striking successes. What's more, continuing design improvements are making these instruments more precise, durable, and affordable. This chapter takes a practical approach to monitoring volcanoes with tiltmeters and strainmeters. For a more thorough treatment of the principles involved, I recommend the review by Agnew (1986).

Broadly speaking, a tiltmeter is any device that can be used to measure changes in the local inclination of the Earth's surface or, in the case of borehole tiltmeters, in the orientation of the borehole. The physical means by which such changes are detected vary widely, and as a result tiltmeters are difficult to classify. One useful distinction that I adopt here from Agnew (1986) is between short- and long-base instruments. The former use a pendulum or bubble as their vertical reference, while the latter use the free surface of a liquid as a horizontal reference. Short-base tiltmeters generally are more portable and less expensive, making them better suited to most volcano crisis responses, although long-base tiltmeters are considerably more precise. Rather than describe the many types of tiltmeters with similar applications, I focus on three that have been used to monitor volcano deformation in a variety of settings worldwide.

3.2.1 Short-base bubble tiltmeters

The most widely used instrument for monitoring ground tilts near volcanoes is the bubble tiltmeter. As the name implies, the instrument's sensor includes a bubble in an electrolytic fluid enclosed in a small tube or disk, typically a few centimeters in size. In one common design, three wires are sealed into a bent glass tube to form electrodes (Figure 3.4). The tube is partially filled with an electrolyte (i.e., a fluid capable of conducting an electrical current). The electrolyte completely covers one of the wires, but includes a small bubble into which the other two wires penetrate. When the sensor tilts, movement of the bubble with respect to the wires causes a conductivity change that can be measured electronically. For small tilts, the magnitude of the tilt change is a linear function of the conductivity change. The tilt direction can be determined with two single-axis sensors, typically arranged perpendicular to one another, or a single biaxial sensor in which a bubble is free to move in two dimensions. Interested readers should consult the excellent article by Powell and Pheifer (2000), who provide a thorough discussion of electrolytic tilt sensors, including theory, design, applications, advantages, and limitations.

For Earth-tilt applications such as volcano monitoring, electrolytic bubble tilt sensors are usually mounted either in a platform housing or in a cylinder suitable for installation in a borehole (Figures 3.5–3.7). For engineering applications such as monitoring the structural integrity of dams or buildings, other types of housings sometimes are preferable (e.g., wall-mount or floor-mount designs). In either case, the sensor is arranged as one element in an electronic circuit designed to measure changes in fluid path conductivity within the bubble.

Westphal *et al.* (1983) used an alternating current Wheatstone bridge design with an inexpensive bubble sensor to construct expendable platform tiltmeters that were used to monitor and help predict dome-building eruptions at Mount St. Helens from 1981 to 1986 (Dzurisin *et al.*, 1983). Commercial manufacturers offer similar designs that can be configured for the sensitivity, dynamic range, and mounting scheme required for a particular application. For most volcano-monitoring applications, 10^{-7} sensitivity (0.1 μrad) over 10^3 μrad of dynamic range is adequate and obtainable at reasonable cost. One microradian (μrad) corresponds to a vertical rise or fall of 1 mm over a horizontal distance of 1 km. Platform designs are preferred for crisis responses because they are relatively easy to transport and install. If time and conditions permit, it is advisable to emplace any tilt sensor at least several meters below ground level to mitigate the effects of temperature fluctuations and other environmental changes. At Kīlauea Volcano, Hawai'i, several bubble tiltmeters installed in boreholes up to 7 m deep exhibit submicroradian sensitivity to short-term tilt changes and have proven to be very useful for tracking intrusive and faulting events (Cervelli *et al.*, 2002a,b; 2003).

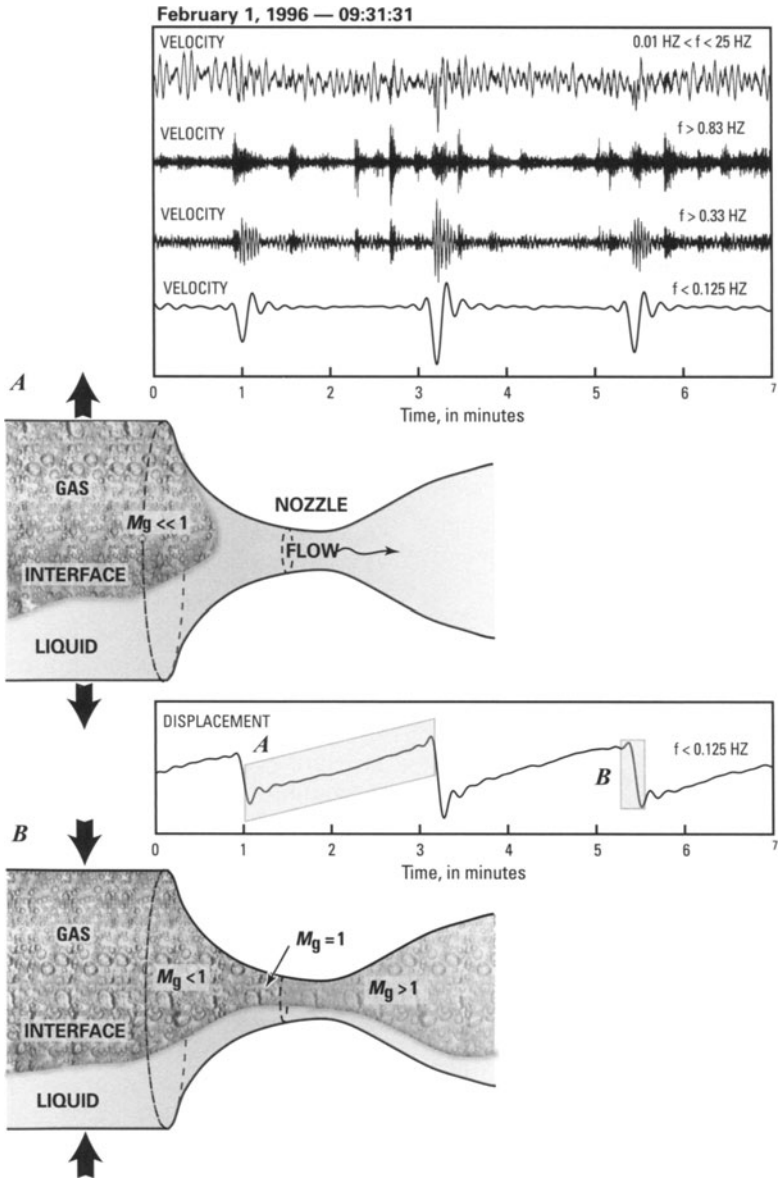

Figure 3.3. Broadband seismic record and associated filtered signals from Kīlauea Volcano, Hawai'i, during a volcanic crisis on 1 February 1996 that included rapid summit inflation, a swarm of VLP earthquakes, and tremor (reproduced from Chouet, 2003, p. 759). *Upper panel* shows the broadband vertical-velocity signal and the same signal filtered in three different frequency (f) bands to produce derivative velocity records for the same 7-minute time interval. Top trace shows the broadband signal ($0.01 < f < 25$ Hz), which is dominated by the oceanic wave-action microseism with periods in the range of 3 to 7 s. Second trace shows the signal after a high-pass filter has been applied ($f > 0.83$ Hz). The result is equivalent to a typical short-period record and shows a series of events superimposed on a background of tremor. Third trace also has a high-pass filter applied ($f > 0.33$ Hz); LP signals with a dominant frequency of about 0.4 Hz are enhanced in this record. Fourth trace shows the signal when a low-pass filter is applied ($f < 0.125$ Hz); in this case, a repetitive VLP signal consisting of pulses with a period of about 20 s ($f \sim 0.05$ Hz) is apparent. Fifth trace (*lower panel*) shows the corresponding displacement record (obtained by integrating the fourth trace above) with a low-pass filter applied ($f < 0.125$ Hz). The displacement record shows a repetitive sawtooth pattern with a rise time of 2–3 minutes and a drop time of 5–10 s. Also shown (lower left, A and B) is a conceptual model of separated gas–liquid flow through a converging–diverging nozzle under choked conditions (after Wallis, 1969, pp. 71–74), which was invoked by Ohminato *et al.* (1998) to explain repetitive VLP signals during the 1 February 1996 crisis at Kīlauea. (A) Inflationary periods lasting 2–3 minutes occur when flow of liquid magma through a constriction in the conduit system blocks the passage of a separate gas phase; these periods correspond to upgoing ramps in the sawtooth displacement record. (B) When the gas pressure upstream of the constriction reaches a critical value, some of the gas slug flows past the constriction, lowering the pressure and re-establishing the initial conditions; these periods correspond to downgoing ramps in the displacement record. The cycle repeats until the magma pressure drops below lithostatic, allowing the constriction to snap shut, and magma transport ceases.

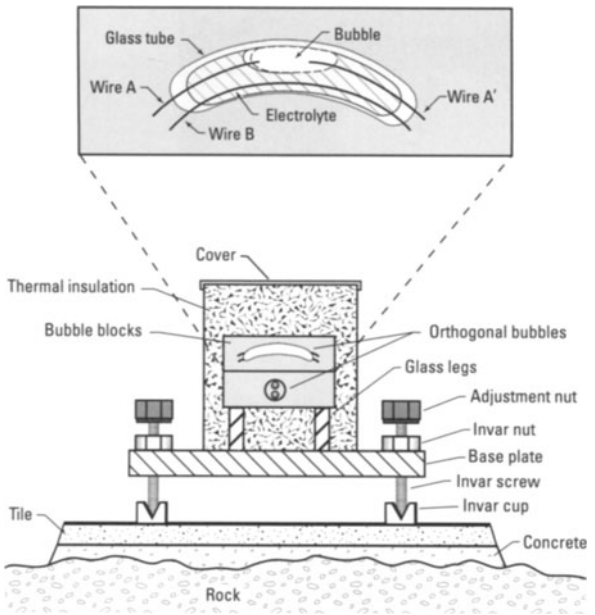

Figure 3.4. Schematic diagram of a typical platform tiltmeter used for volcano monitoring (Westphal *et al.*, 1983). Movement of a bubble (*inset*, dashed line) in an electrolytic fluid causes impedance changes across a glass tube that is part of an electronic impedance bridge. The impedance changes, which are proportional to ground tilt, are sampled periodically (e.g., at 10-minute intervals), converted to a digital signal, and telemetered to a data analysis facility. (*inset*) When the sensor tilts, movement of the bubble with respect to wires A and A causes a change in conductivity of the fluid path between wires A and B and between A and B, which can be measured electronically and related to the tilt in the direction of the long axis of the tube. Two sensors arranged perpendicular to one another measure two orthogonal tilt components, thus determining the resultant tilt vector. Platform tiltmeters can be installed on the surface, but a better approach is to isolate them from small-scale, near-surface effects by anchoring them securely in a tunnel or vault.

3.2.2 The Ideal-Aerosmith mercury capacitance tiltmeter

The Ideal-Aerosmith mercury capacitance tiltmeter near the summit of Kīlauea Volcano, Hawai′i, illustrates the utility of short-base electronic tiltmeters for monitoring ground deformation at active volcanoes. At each end of a 1-m-long tube, a pool of mercury is separated from a metal plate by an airspace gap, forming a parallel-plate capacitor.[16] A second tube filled with air, which is sealed from the atmosphere, also connects the pools. As the instrument tilts, mercury flows through the first tube from one pool into the other to maintain hydrostatic equilibrium, thereby changing the capacitances. The capacitance change is sensed electronically with an electronic bridge circuit, converted to the equivalent tilt change, and recorded at the nearby United States Geological Survey (USGS) HVO. The instrument, which has short-term sensitivity of ~0.1 μrad, was installed in Uwekahuna Vault in 1965 and was still operational in 2006.

Records from the Uwekahuna Ideal-Aerosmith tiltmeter for the early parts of two long-lived eruptions along Kīlauea's East Rift Zone demonstrate the instrument's capability (Figure 3.8). At Mauna Ulu in 1969 and again at Pu′u ′Ō′ō in 1983–1984, eruptive episodes ranged in duration from hours to several days and were characterized by high-volume discharge of lava flows, vigorous lava fountaining, rapid summit subsidence, and strong harmonic tremor in the vent area. Recurring tilt patterns like those in Figure 3.8 led Dvorak and Okamura (1987) to propose a hydraulic model to explain variations in the tilt rate during summit subsidence events. They assumed that: (1) the magma flow rate is proportional to the pressure difference between the summit reservoir and a separate reservoir or series of reservoirs within the rift system, and (2) magmatic pressure is linearly related to volumetric strain. It follows that the magma flow rate and, hence, the summit tilt curve will follow an exponential decay. Dvorak and Okamura (1987) showed that the exponential curve represented by $\tau = 32 \times (1 - e^{-t/40})$, where τ represents the summit tilt value in microradians as a function of time t in days, fits the Ideal-Aerosmith record for episodes 2–9 of the Pu′u ′Ō′ō eruption remarkably well (Figure 3.9).

3.2.3 Long-base fluid tiltmeters

In situations where volcanic unrest may continue for several years, expected tilts are small, and adequate resources are available for monitoring, long-base fluid tiltmeters are preferable over short-base

[16] A capacitor stores energy in the electric field created between a pair of conductors on which equal but opposite electric charges have been placed; a simple design consists of two parallel, electrically conductive plates connected to a battery or other power source. For a *parallel-plate capacitor*, capacitance C is directly proportional to plate area and inversely proportional to plate separation. Furthermore, $C = Q/V$, where Q is electric charge and V is potential difference (voltage). A change in capacitance caused, for example, by a change in plate separation produces a corresponding change in Q/V, which can be measured electronically. In the Ideal-Aerosmith mercury capacitance tiltmeter, tilting of the ground surface produces a change in plate separation (capacitance) in an electronic sensing circuit.

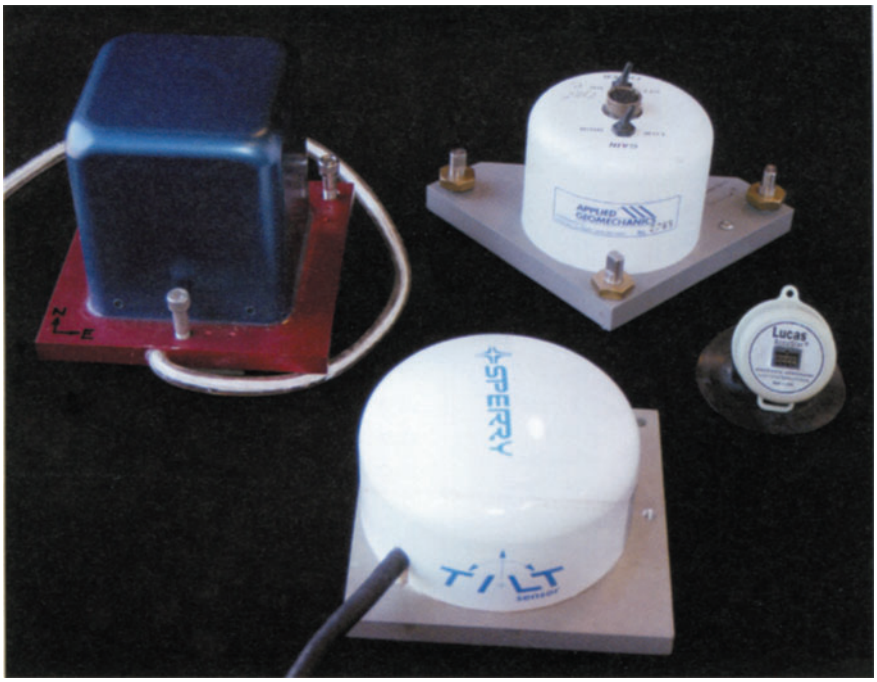

Figure 3.5. Four examples of platform tiltmeters suitable for volcano monitoring, including three from commercial suppliers and one prototype (*upper left*) that was designed and built specifically for use in the 1980 crater at Mount St. Helens (Westphal *et al.*, 1983; Dzurisin *et al.*, 1983). The 'Westphal tiltmeter' was an interim response to frequent dome-building episodes at Mount St. Helens during 1980--1986, which created a need for robust, relatively inexpensive, 'expendable' monitoring instruments. The small tiltmeter on the right (~5 cm in diameter) is designed for mounting on a vertical surface such as a rock wall; the other three are for use on a horizontal surface. Such designs are generally susceptible to thermal and other near-surface environmental effects that can be reduced substantially by installing them a few meters underground (e.g., in a vault or tunnel). USGS photograph by David E. Wieprecht.

designs. This is because long-base instruments generally are more precise and less susceptible to small-scale tilt fluctuations (i.e., 'noise' associated with localized ground movements that can be caused by differential settling, rain or snow loading, freeze/thaw cycles, etc.) than their short-base counterparts (assuming careful installation of the long-base piers). The best long-base tiltmeters are hundreds of meters long and have sensitivity on the order of one part per billion (10^{-3} μrad). Such instruments easily resolve the solid Earth tide ($\sim 10^{-1}$ μrad), which can be computed accurately from theory and removed from the tiltmeter record. Because they are expensive and require elaborate installations and maintenance to isolate them from surface environmental effects, they are best suited to persistently active volcanoes where the threat to lives and property is high.

As is the case for short-base tiltmeters, long-base tiltmeters are available in a wide variety of designs. Most include one or two tubes at least 100-m long and either filled or partly filled with a liquid, usually water. Sensors at each end of the tube(s) measure the height of the liquid surface with respect to some reference point tied to the ground. The liquid surface remains horizontal as the tube tilts, resulting in relative surface-height changes between the ends of the tube(s). These changes can be measured with various types of sensors, including a micrometer, pressure transducer, or interferometer, to determine the magnitude and, for biaxial designs, the direction of tilt (Agnew, 1986) (Figure 3.10).

Tubes that are completely filled with liquid are easier to install, because they don't have to be precisely level, but they are sensitive to slight environmental differences that are hard to eliminate along their entire length (e.g., temperature or pressure differences between the ends of the tube cause surface-height differences that are unrelated to ground tilt). An early implementation of this approach was the so-called wet tilt method developed by Eaton (1959) at the USGS HVO. In 1958, Eaton and the HVO staff installed 10 long-base watertube tiltmeters around the summit of Kīlauea Volcano (Yamashita, 1992). The installations consisted of three sunken concrete piers, each with a brass

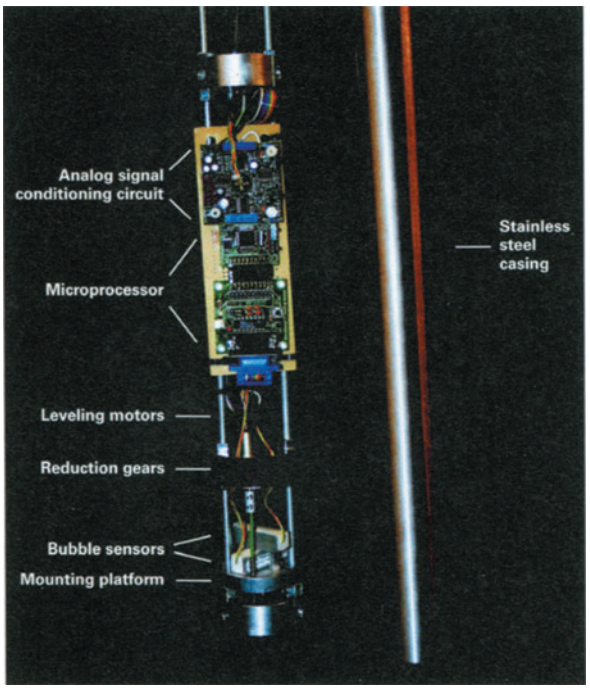

Figure 3.6. Dual-axis borehole tiltmeter design by Richard G. LaHusen, USGS. Analog and digital electronics are located downhole to avoid surface thermal effects. Leveling motors and reduction gears are operated by the microprocessor to re-level the mounting platform and its bubble sensors when the inclination exceeds full-scale range. Re-leveling can be accomplished either automatically or remotely via telemetry links. The tiltmeter package is housed in a submersible, 214 inch (55 mm) diameter stainless steel casing. Tiltmeter can be permanently grouted or temporarily set in sand within a 3-inch (75-mm) drill hole. USGS photograph by David E. Wieprecht.

container (pot) attached. The pots were machined from spent artillery shells, which were in abundant supply at a nearby military base. Each pair of pots was connected by a water hose and an air hose. The water hose was used to fill the pots and allow water to flow freely between them until equilibrium was reached. The air hose assured equal pressure between the pots. Micrometers were used to measure the height of the water in all three pots simultaneously, so the elevation differences between the piers could be calculated precisely.

Such installations were possible only where the elevation difference between the piers was no greater than 1.5 cm (the effective range of the micrometers) in an equilateral triangle with 20–50 m sides. The highest precision could be obtained only at night in fog or under heavy cloud cover, owing to thermal expansion or contraction of the water in the system during daylight hours. Because water was used as the medium to determine the elevation differences between the piers, and also because of the environmental conditions that were most conducive to good measurements, the term 'wet tilt' was applied to the method. Although no longer used at HVO, the simplicity of the wet tilt method was attractive to volcanologists elsewhere and it still is being used to monitor a few of the world's volcanoes. Another part of its continuing legacy is the term 'dry tilt,' which was coined at HVO to distinguish single-setup leveling (Section 2.5.2) from the wet tilt technique.

The shortcomings of water-filled tubes can be mitigated further by using a partly filled tube, which constitutes a miniature lake with an equipotential surface. Precision on the order of 1 nanoradian (10^{-9} rad or 10^{-3} μrad) can be achieved by burying such a device or installing it in a tunnel to insulate it from temperature fluctuations. Care must be taken to ensure that the tube is precisely level so a mini-lake can be maintained within it. This requires either a carefully constructed trench or an accessible tunnel, which can be hard to come by near an active volcano.

A biaxial long-base tiltmeter at the Long Valley Caldera in California uses two orthogonal tubes, 423 m and 449 m long, which are half-filled with water and buried at a mean depth of 1.5 m (Behr *et al.*, 1992). The water level is measured at the ends of the tubes by laser interferometer transducers. Each transducer has a water-height resolution of approximately 0.25 μm, which corresponds to a tilt resolution of 0.6 nanoradians (0.0006 μrad). The ends of the tiltmeter are referenced to points 20-m deep by 3 borehole extensometers with displacement resolution of about 0.05 μm. After correction for atmospheric pressure variation, thermal expansion, and surface displacements, the instrument shows a long-term stability on the order of 0.1 μrad yr^{-1}. Such an elegant device is unaffordable or not feasible at most volcanoes, but in special cases its high precision and low drift rate can provide unique insights into magmatic processes. This is especially true if the strain rate is low but volcanic risk is high (e.g., relatively deep or gradual magma intrusion near a population center).

Another noteworthy long-base tiltmeter for volcano monitoring is installed in a tunnel 2.8 km northwest of the summit crater at Sakurajima Volcano in southern Japan (Kamo and Ishihara, 1989). The site was located at this distance to measure the maximum tilts expected from pressure changes in a magma source at 3–5 km depth beneath the crater, as revealed by repeated leveling surveys. To isolate the instrument from surface

Figure 3.7. Scientists install a shallow-borehole tiltmeter (~2-m) on the September 1984 lobe (foreground) of the 1980–1986 lava dome at Mount St. Helens, Washington. An active spine of the 2004–2006 lava dome, ~ 400 m distant, is visible near the upper left corner of the large photo, in front of the 1980 crater wall and rim on the skyline. View is to the south. A steel casing is hammered and cemented to the bottom of an 8 cm (3 inch) diamter drill hole (large photo). The tiltmeter is lowered to the bottom of the casing (*inset*, lower left) and secured with fine sand. The upper part of the casing is covered with a short section of PVC plastic pipe (*inset*, lower right); cables connect the tiltmeter to electrical power (solar panel and high-capacity rechargeable baterries) and a radio telemetry system (not shown). USGS photographs by Daniel Dzurisin, 5 August 2005.

environmental effects, a tunnel was constructed in the Harutayama lava dome specifically for this purpose, and a biaxial watertube tiltmeter and 3-component extensometer were installed in 1985. The watertube is 28 m long and 15 mm in diameter with water reservoirs at each end. Water levels are detected by a float in each reservoir and transformed into an electrical signal by a magnetic sensor. Inflationary radial tilt in the range from 0.01 μrad to 0.2 μrad is observed consistently for periods of 10 minutes to 7 hours prior to explosions in the summit crater. These episodes are followed by periods of deflation by approximately the same amount (Figure 3.11).

In an experiment to test an automated warning system based on the tiltmeter signal, scientists defined five stages of eruptive activity (ongoing eruption, non-eruption, pre-eruption, warning, and critical) and used a computer to determine the stage in real time (Figure 3.11). During a 25-day experiment in 1985, there were 39 explosions. All but one occurred during pre-eruption or further advanced stages. The computer reported 59 critical stages, 38 of which correspond to eruptive events. The other 21 critical stages were not accompanied by significant eruptive activity. Most of these 'false alarms' were caused by temporary deflations associated with minor eruptions or gas emissions (Kamo and Ishihara, 1989). This was a pioneering experiment that led to significant improvements in the system, and now residents are accustomed to receiving accurate, automated, short-term warnings before most of Sakurajima's hazardous eruptions.

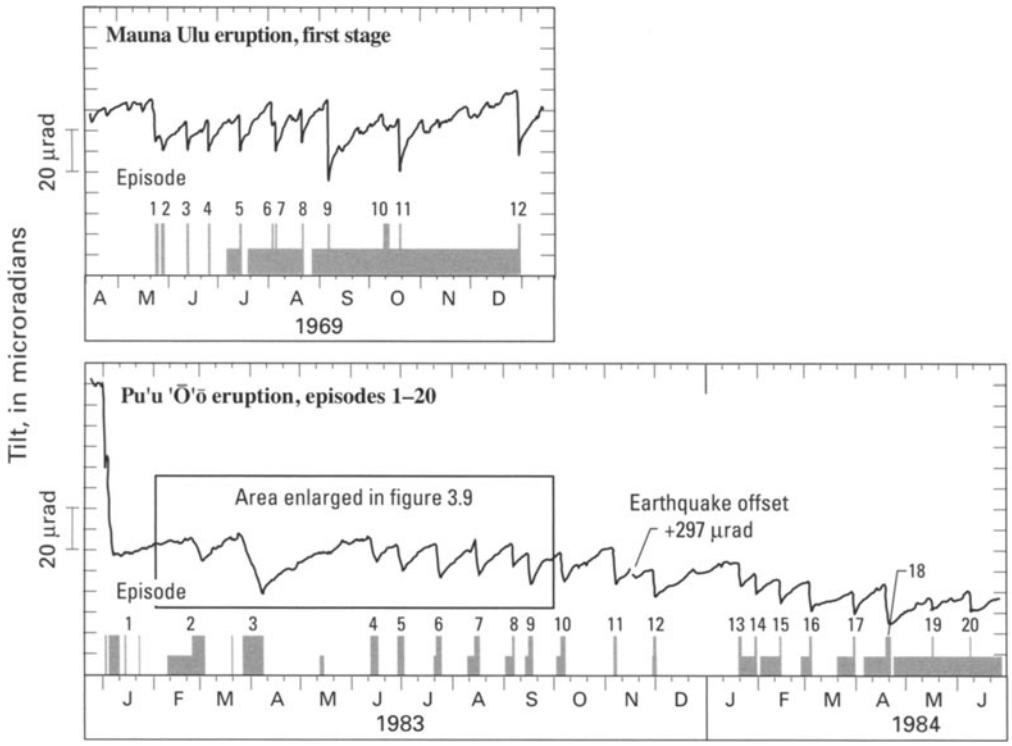

Figure 3.8. West–east tilt records from the Ideal-Aerosmith mercury capacitance tiltmeter, which has been housed in Uwekahuna Vault near the summit of Kīlauea Volcano since 1965, for parts of two long-lived eruptions along the East Rift Zone (Wolfe *et al.*, 1987). Full-height bars represent eruptive episodes that were characterized by high-volume discharge of lava flows, vigorous lava fountaining, rapid summit subsidence, and strong harmonic tremor in the vent area. Half-height bars represent periods low-volume effusive activity at the vent during reposes between high-fountaining episodes.

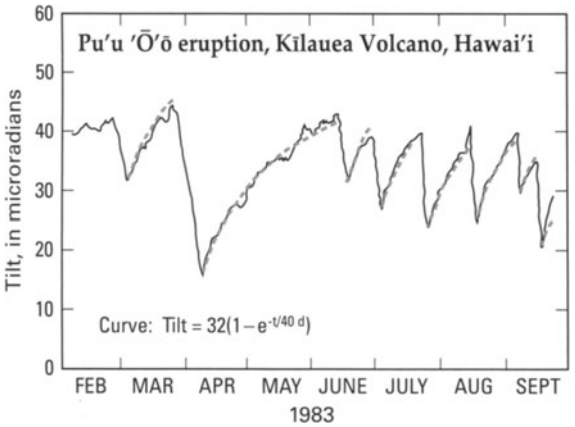

Figure 3.9. West–east tilt changes recorded from February to September 1983, which included episodes 2--9 of the Pu'u 'Ō'ō eruption along Kīlauea's East Rift Zone, by the Ideal-Aerosmith tiltmeter at Uwekahuna Vault in the summit area (Dvorak and Okamura, 1987). Periods of increasing tilt values correspond to summit uplift and magma accumulation beneath the summit area; periods of rapidly decreasing tilt values correspond to magma withdrawal from beneath the summit area and vigorous eruptive activity along the rift zone. The same exponential curve, for a maximum tilt change of 32 µrad and a time constant of 40 days, is fit empirically to all eight periods of summit uplift.

3.3 STRAINMETERS

Strain is loosely defined as a change in the volume (dilation) or shape (distortion) of a body as a result of stress, expressed as a dimensionless ratio: $\varepsilon = p_1/p_0$, where p_1 and p_0 represent final and initial states, respectively. Such a change implies relative displacements among the body's parts, and, in the most general case, these occur in three dimensions. Under the assumption of uniform strain throughout the body, we can write a strain tensor that relates the body's final state to its initial state by specifying the vector displacements of any part along three orthogonal axes. It follows that, for convenience, we can consider the linear strain l_1/l_0, surface strain s_1/s_0, or the most general case of volumetric strain v_1/v_0. In practice, most strainmeters are designed to measure either linear strain or volumetric strain. The first type is useful when strain is known to be localized and dominantly 1-D (e.g., across a narrow linear zone of surface extension or contraction), while the second type provides valuable information about

spatially distributed strain changes caused by such processes as magmatic inflation or intrusion.

3.3.1 Linear strainmeters (extensometers)

Linear strainmeters are designed to measure the displacement between two separated points, either on the surface or in a borehole. The most common types of linear strainmeters are rod strainmeters, wire strainmeters, and laser strainmeters. Invar-rod and Invar-wire strainmeters used to monitor creep along the San Andreas Fault in central California have resolutions of 0.05 mm and 0.02 mm, respectively. Laser strainmeters are capable of fantastic precision, on the order of 10^{-10} to 10^{-13} (100 to 0.1 parts per trillion) (Agnew, 1986), but their complexity and high cost make them unsuitable for most volcano-monitoring applications. Because all designs are susceptible to environmental effects such as temperature fluctuations and loading by rain or snow, careful attention must be paid to isolating the strainmeter from such effects (e.g., by installing the instrument in a tunnel, burying it, or providing a sturdy insulated housing). Another important consideration is the means by which the strainmeter is attached securely to the ground. This is best and most easily accomplished by anchoring in bedrock, but where none is available, anchor rods driven to refusal may suffice. Deeply anchored piers isolated from surface movements are preferable to surface or shallow piers. Common sense, practicality, and budget are the best guides in this regard.

As the name implies, rod strainmeters use a solid rod to detect the relative displacement between two piers that are well anchored to the ground. One end of the rod is attached to one of the piers and the other is attached to a digital caliper or similar device, which is attached to the second pier. The rod transfers any relative displacement between the piers to the displacement sensor, which measures it; the result is recorded on site or telemetered to an analysis facility. If strain is distributed across a wide zone that can't be entirely spanned by the strainmeter,

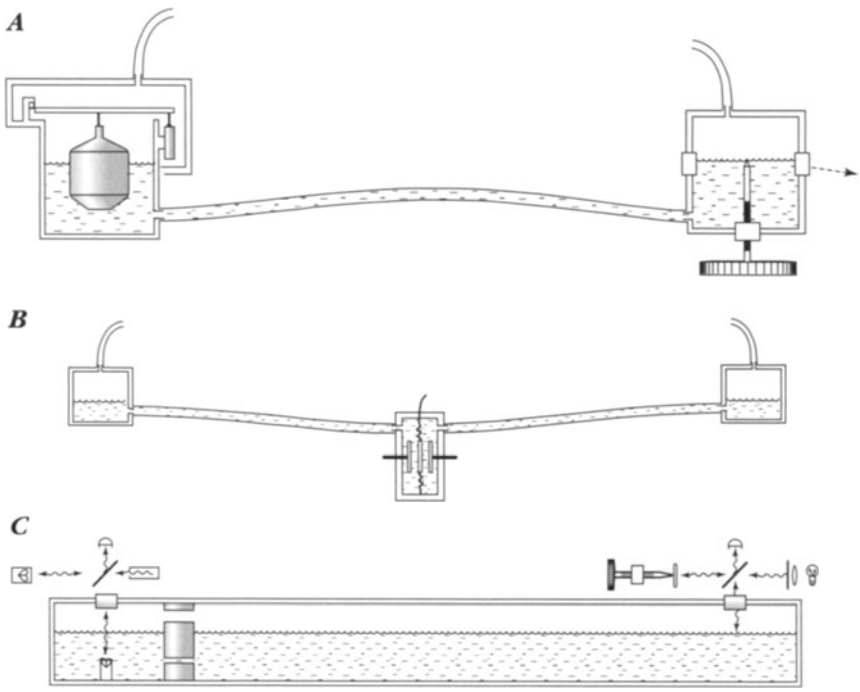

Figure 3.10. Three different designs of long-base tiltmeters (Agnew, 1986). For greater completeness, different types of sensors are shown at the two ends of each tiltmeter in A and C, though in reality such instruments are symmetric. (A) Pot-and-tube tiltmeter with (*left*) a typical design of float sensor and (*right*) a visually read micrometer. (B) Center-pressure tiltmeter with a pressure transducer to measure relative height changes. (C) Michelson-Gale tiltmeter, with (*left*) a laser interferometer and (*right*) a white-light interferometer used to measure the liquid level. A key feature of this design is that the tube is only half-filled with liquid, which ensures an equipotential surface. A biaxial instrument capable of determining tilt direction can be made by adding a second tube, usually perpendicular to the first, and a third sensor.

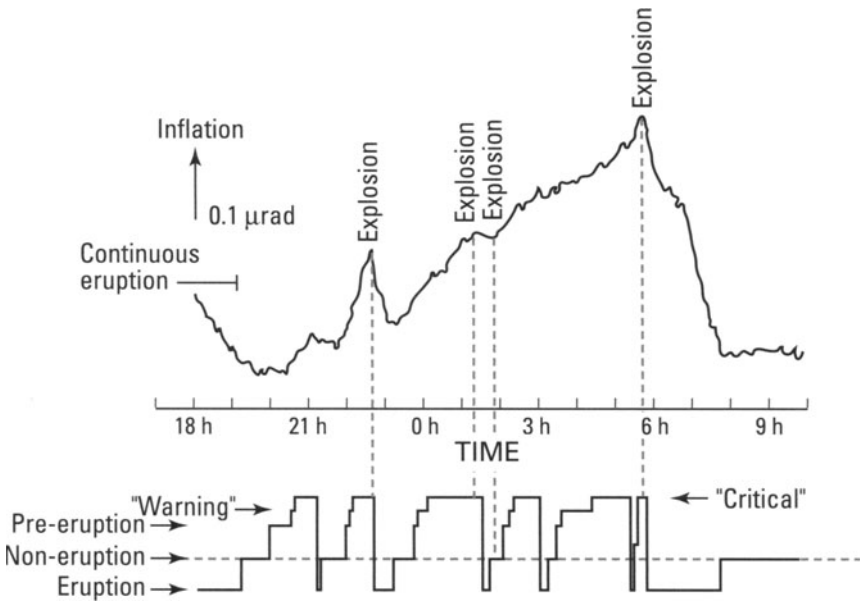

Figure 3.11. Radial tilt record for a 16-hour period on 18--19 December 1985, from a 28-m biaxial watertube tiltmeter in a tunnel near the summit crater of Sakurajima Volcano, Japan (Kamo and Ishihara, 1989). Also shown (*bottom*) are results of an experiment in which the tiltmeter record was used to automatically assign an activity stage in near-real time, according to a five-level scheme from 'ongoing eruption' (lowest alert) to 'critical.' See text for discussion.

wider spacing between the piers (i.e., using a longer rod) generally is a good idea, because the resulting signal at the displacement sensor is larger. This leads to a trade-off between portability and sensitivity. A longer rod captures more displacement, but is less portable than a shorter rod. For a given displacement sensor, sensitivity to small strains is greater with a longer rod. If displacement is known to be localized, (e.g., across a fault or crack), then a rod strainmeter long enough to span the feature is a good choice. Bilham (1989) used a ~1 cm diameter Invar rod, 6–7 m long, encased in a flexible lubricated tube to monitor creep at the Superstition Hills Fault in southern California. The equipment has sensitivity of 10 μm and therefore can detect a strain change of 1.7 μstrain over the instrument's length.

Where a longer reach is desired, a flexible wire sometimes provides a good alternative to a rigid rod. A wire stretched across a crack or deforming arca, fixed to the ground at one end and attached to a displacement sensor at the other, can be very effective. For example, Iwatsubo *et al.* (1992b) used such an arrangement to monitor changes in the widths of radial cracks adjacent to a growing dacite dome at Mount St. Helens. Experience had shown that crack widening by several centimeters or more was likely in the days leading up to an extrusive episode, and that monitoring stations near the dome were likely to be damaged or destroyed by repeated eruptive activity. Therefore, sophisticated strainmeter installations were impractical and not cost-effective. Instead, a relatively inexpensive ($500) commercial displacement meter with a stainless steel wire a few meters long was stretched between two 2-m steel fence posts driven into the ground and cemented on either side of a crack (Figure 1.22). The displacement meter used a potentiometer and battery to convert linear displacement to an electrical signal, which was digitized and telemetered to the USGS David A. Johnston Cascades Volcano Observatory (CVO), 70 km away in Vancouver, Washington. With a 3.8 m long wire, 12-bit analog-to-digital converter, and low-data-rate digital telemetry system (Murray, 1992), these homebuilt strainmeters could resolve crack displacements as small as ~1 mm – more than adequate for the task at hand. A wooden or metal conduit was used to protect the wire from heavy winter snow pack and other environmental hazards such as falling rocks and tephra. Starting about 6 days before an extrusive episode in May 1985, one such strainmeter recorded ~10 cm of extension across a radial crack in the crater floor near the base of the dome, which aided in a successful prediction of the event.

3.3.2 The Sacks–Evertson volumetric strainmeter

Most forms of solid-body deformation involve volumetric strain (i.e., an increase or decrease in volume (dilatational or compressional strain, respectively)). This type of strain is especially important in volcanology, because it commonly occurs as a result of magma movement, inflation or deflation of a magma reservoir, or pressure changes in a magma body or hydrothermal system. An elegant means to measure volumetric strain was first proposed by Benioff (1935), who suggested burying a large container of fluid with a small opening (akin to a sealed plastic bottle containing a narrow soda straw). Strains in the ground would change the volume of the container and force fluid to flow in or out of the straw. The narrower the straw, the farther a given volume of liquid (corresponding to a given change in volumetric strain) would move up or down inside the straw. By sensing the position of the liquid column in the straw, a precise measurement of volumetric strain could be obtained.

This principle was put into practice by I.S. Sacks and D.W. Evertson, who designed a remarkably sensitive instrument suitable for installation in a borehole (Sacks *et al.*, 1971; Figures 9.1 and 9.2). It is essential that such a precise instrument be installed in a borehole, preferably 200 m or more deep, to isolate it from spurious strains caused by environmental fluctuations near the surface. The Sacks–Evertson volumetric strainmeter and some of its applications to volcano monitoring are more fully described in Chapter 9, which deals specifically with borehole observations of strain and fluid pressure.

Sacks–Evertson strainmeters installed in California during the 1980s and 1990s, including four in the Long Valley region, have sensitivities on the order of 10^{-12} (one part per trillion) over periods of seconds to minutes. Instrumental drift and other factors (e.g., imperfect coupling to the host rock by means of an expanding grout, which creates strain as it hardens and cures) affect longer term signals to the extent that such minuscule strains cannot be resolved. Nonetheless, experience shows that the instruments are capable of resolving strain changes of 5×10^{-9} over periods of a few hours to a few days (Johnston *et al.*, 1994). Such high sensitivity means that interesting signals can be recorded much farther from the source than is possible with most other instruments. For volcano monitoring, this translates into safer and more sensitive monitoring stations farther from the volcano – an important factor for working under hazardous conditions. On the other hand, the need to install this type of strainmeter in a relatively deep borehole, which is expensive and time-consuming to drill, makes it poorly suited for most volcano emergency responses.

Sacks–Evertson strainmeters have been installed near several volcanoes around the world, including Hekla Volcano, Iceland. Five of the instruments recorded remarkably similar sets of strain signals associated with explosive eruptions in 1991 and 2000. In the latter case, a warning based on the strain and seismic data was issued about 20 minutes before the eruption began (Agustsson *et al.*, 2000). This feat is all the more remarkable because four of the strainmeters are located more than 35 km from the volcano (Section 9.5.3). That's farther than the distance from the summit of Kīlauea to the summit of Mauna Loa, Hawai'i, and about halfway to Portland, Oregon, from Mount St. Helens, Washington! Tempering the excitement, however, is the fact that anomalous strain signals were recognized only about 30 minutes before the Hekla eruptions began – which leaves scant time for warning and response.

When and how magma accumulates before explosive eruptions, especially before the onset of precursory earthquakes, is a key question to be addressed by future volcano-monitoring efforts and theoretical studies. If magma accumulation beneath hazardous volcanoes can be detected months or even years before an eruption, reasonable steps can be taken well in advance to mitigate the eruption's social and economic impact. If, on the other hand, substantial volumes of magma can accumulate in the middle to upper crust and escape detection, even by the most sensitive instruments available, volcano hazards mitigation will continue to present a much greater challenge. Even in the first, more optimistic scenario, determining whether magma accumulation will culminate in a hazardous eruption or a relatively benign intrusion is likely to be extremely difficult for the foreseeable future.

Consider the dilemma posed by recent experiences at Redoubt Volcano in Alaska (1989), Hekla (1991), and Rabaul Caldera in Papua, New Guinea (1994). At Redoubt, more than two decades of repose ended suddenly with a large explosive eruption that began on 14 December 1989 (Brantley, 1990). In hindsight, volcanologists learned that a pilot flying near the volcano on 20 November had noticed a small white 'cloud' rising a few hundred meters above the summit crater and a strong sulfur odor downwind from

the volcano. Additional pilot reports of small steam plumes were received on 3 December and 8 December. On 13 December, small earthquakes began to be recorded beneath the volcano at a rapidly increasing pace by a network of seismometers that included three geophones within 15 km of the summit (Power *et al.*, 1994). Most of the earthquakes were located within 2 km of the surface and none was as large as M 3. The eruption began explosively just 24 hours after the first detection of unusual seismic activity. A collection of papers edited by Miller and Chouet (1994) provides a comprehensive account and analysis of the 1989–1990 eruption sequence at Redoubt.

The Redoubt experience left room for hope that a denser local seismic network or other monitoring techniques (e.g., continuous geodetic or geochemical measurements) might have provided a longer term warning. This optimistic view, however, seems to run contrary to experience at Hekla in 1991 and 2000. Had a similar eruption occurred in a populated area with very little warning, the consequences could have been severe. Hekla might be unusual in this regard, because there are many examples of volcanoes that inflate gradually over a long time and thus provide ample warning before eruptions. On the other hand, for the subset of historical eruptions with a paroxysmal event of Volcanic Explosivity Index (VEI) ≥ 3 ($>10^7$ m^3 of tephra, cloud column height >3 km, and described as 'severe' or 'violent'), in 45% of the cases the paroxysm came within the eruption's first day. Furthermore, half of the first-day paroxysms came within the eruption's first hour (Simkin and Siebert, 1984, pp. 112–113).

Rabaul Caldera is one example of a magmatic system that inflated gradually for many years before its 1994 eruption, but experience there offers scant comfort. Were it not for a comprehensive volcano hazards mitigation plan developed over more than two decades of sporadic unrest, and also for the resourcefulness of local residents who self-evacuated in accordance with the plan when the situation worsened to critical in just a matter of hours, thousands might have lost their lives in spite of an intensive monitoring effort. Here the problem was not a lack of intermediate-term precursors. On the contrary, repeated seismic swarms and broad uplift of the caldera floor began in 1971, increased dramatically in 1983, and continued to fluctuate in intensity until the early morning hours of 18 September 1994 (Newhall and Dzurisin, 1988, pp. 219–240). Then, in just 27 hours, the level of activity intensified abruptly from background (very low at the time) to simultaneous eruptions at two sites along the caldera rim, Vulcan and Tavurvur Volcanoes, which had not been active since 1937–1943 (McKee *et al.*, 1995; Blong and McKee, 1995; Lauer, 1995). Of course, longer term warning might have been possible if sensitive tiltmeters or strainmeters had been operating in the area, but there is no way to be sure. Sadly, there seems to be no guarantee of more than a few hours warning before some eruptions, even at well-monitored volcanoes.

In summary, volumetric strainmeters have the potential to significantly improve our ability to safely monitor crustal deformation caused by volcanic processes, especially if the instruments' size and installation cost continue to shrink. The two issues are related, because the cost of boring a hole is a significant fraction of the total installation cost, and small-diameter drill holes are much less expensive than large ones. Reducing the average installation cost would go a long way toward addressing two concerns that have delayed the instruments' widespread acceptance within the volcanological community. First is the potential for installation failures, especially failure to couple the strainmeter adequately to the wall of the borehole. Unfortunately, such flawed installations are permanent, rendering the instrument essentially useless. Of course, their adverse impact on a volcano-monitoring budget decreases in proportion to the shrinking installation cost. A second impediment to widespread use of volumetric strainmeters for volcano monitoring is the fact that a single strainmeter cannot provide directional information (unlike a tiltmeter, for example). This means that several strainmeters must be deployed in an array in order to locate and monitor a deformation source. Multiple-sensor arrays are always wise, but the relatively high cost of strainmeters has, in the past, caused most volcano observatories to opt for less expensive, less sensitive deformation sensors. If this obstacle can be overcome, perhaps through design changes that reduce cost while maintaining an adequate level of strain sensitivity, volumetric strainmeters likely will be deployed at many more volcanoes in the coming decades.

3.3.3 The Gladwin tensor strainmeter

Although it was designed primarily for mining and tectonic applications, the Gladwin tensor strainmeter (Gladwin, 1984; Gladwin and Hart, 1985) or some variation thereof might also see expanded use at volcanoes in the near future. Like the Sacks–

Evertson dilatometer, the tensor strainmeter is intended for installation in a borehole, preferably 200 m or more deep. Unlike the dilatometer, which measures volumetric strain (a scalar quantity), the tensor strainmeter determines the three independent components of the surface strain field, $\varepsilon_{xx}, \varepsilon_{yy}, \varepsilon_{xy}$.[17] For an isotropic material, the 3-D strain tensor generally has six independent components. Near the surface of the Earth, however, vertical stress and tractions are zero, so the strain field is completely described by three horizontal components.

The Gladwin tensor strainmeter uses three horizontal extensometers arranged vertically in a cylinder, each rotated 120° with respect to its neighbor, to measure the three independent components of horizontal strain. Each transducer consists of a three-plate capacitor. The plates are attached to the walls of the cylinder in such a way that deformation of the cylinder wall is transferred effectively to the gaps between plates. The resulting differential capacitance changes are measured with an electronic bridge circuit specially designed for high sensitivity and electronic stability. Strain sensitivity is on the order of 10^{-11} and the instrument's frequency response is flat from 0 Hz to more than 10 Hz. This means that the instrument is equally well suited to measuring gradual strain accumulation, such as might be caused by magmatic inflation, as well as much higher frequency strains associated with volcanic earthquakes and fluid flow, for example.

Tensor strainmeters of this type have been installed in mines since the late 1960s and near active faults since the early 1980s. Three were installed in 1986 along a creeping section of the San Andreas Fault near Parkfield in central California. Starting in mid-1993, two of those instruments detected a significant change in the accumulation rate of shear strain (0.5 and 1.0 microstrain per year). The third instrument also detected a change, but it is affected by localized deformation due to hydrology and, therefore, its data were discounted (Gwyther *et al.*, 1996). The strain-rate change, which was corroborated by two-color electronic distance meter (EDM) measurements, coincided with two other notable events. High rainfall in early 1993 ended a seven-year period of subnormal precipitation, and from late 1992 through late 1994 the Parkfield region had an increase in the number of magnitude 4–5 earthquakes relative to the preceding six years. Gwyther *et al.* (1996) and Langbein *et al.* (1999) recognized that the strain-rate change could have been induced by rainfall, but concluded that the more likely explanation is a change in the rate of aseismic slip on the San Andreas Fault at depth.

Tensor strainmeters are an integral part of the Plate Boundary Observatory (PBO), a state-of-the-art geodetic facility funded by the National Science Foundation (U.S.A.) to study deformation across the boundary zone between the Pacific and North American plates. Field operations commenced in 2004 and by the end of this decade PBO plans to install up to 175 Gladwin-type strainmeters and 875 continuous GPS (CGPS) stations in the western U.S.A., including instrument clusters at selected volcanoes in the Aleutians and Cascades, Yellowstone, and Long Valley (Section 4.10.3).

3.4 CONTINUOUS GPS

CGPS stations, which are set up to operate autonomously for long periods of time, have several advantages over repeated, campaign-style GPS surveys for volcano monitoring (Chapter 4). So-called 'permanent' CGPS stations include provisions for long-term power (typically a combination of batteries and solar panels at remote sites) and telemetry (radio, phone, or Internet). Therefore, they provide a continuous real-time data stream that can be analyzed either immediately using predicted satellite orbits or later using more precise orbits to obtain a record of 3-D surface displacement as a function of time.

An obvious advantage of this approach is the ability to track transitory deformation events such as the passage of a dike in near-real time. Once a network of CGPS stations is established, its maintenance requirements usually are lower in terms of field personnel than for repeated campaign-style surveys. Continuous records also offer an opportunity to recognize immediately such short-term deformation events as slow earthquakes, which might otherwise go unnoticed or be recognized only after the fact (Dragert *et al.*, 2001; Crescentini *et al.*, 1999; Linde *et al.*, 1996; Kawasaki *et al.*, 1995). Such

[17] For isotropic materials, the strain tensor is a symmetric second-rank tensor (i.e., a 3×3 matrix in which $\varepsilon_{ij} = \varepsilon_{ji}$ for $i, j = 1, 2, 3$) used to quantify the strain of an object undergoing a 3-D deformation. In general, six quantities are required: 3 diagonal terms to specify the relative changes in length along 3 orthogonal axes (principal strains ε_{11}, ε_{22}, and ε_{33}), and 3 off-diagonal terms to specify changes in the object's shape (shear strains $\varepsilon_{12} = \varepsilon_{21}$, $\varepsilon_{13} = \varepsilon_{31}$, and $\varepsilon_{23} = \varepsilon_{32}$). Volumetric strain is equal to the trace of the strain tensor: $\Delta V/V_0 = \varepsilon_{11} + \varepsilon_{22} + \varepsilon_{33}$. The Sacks--Evertson dilatometer measures the scalar quantity $\Delta V/V_0$, whereas the Gladwin tensor strainmeter determines ε_{11}, ε_{22}, and ε_{12} separately.

events have been observed recently for the first time at the Long Valley Caldera and Kīlauea Volcano by CGPS and borehole dilatometers. The mechanism of slow earthquakes at volcanoes is not yet understood, but their discovery lends credence to the idea that the closer we look at deforming volcanoes in space and time, the more we see.

A disadvantage of CGPS is that each receiver is tied to a single location rather than being available for re-location within a network of stations, as is the case for campaign-style surveys. Combined with the inevitable limitations on funding, this means that the spatial density of CGPS networks is often suboptimal (i.e., we can afford many fewer stations than we need). In addition, CGPS stations are subject to spurious environmental effects that plague all near-surface geodetic sensors. For CGPS, these include small movements induced by diurnal or seasonal temperature fluctuations, surface loading by precipitation, phase-center shifts caused by snow accumulation on the GPS antenna, and even such mundane annoyances as disturbance by animals, theft, or vandalism. On the other hand, the cost of GPS hardware and telemetry is continuing to decline as the utility of CGPS for a wide variety of applications becomes apparent. As a result, reasonably dense networks of 10–20 CGPS stations have been established at Kīlauea Volcano, Hawai'i (Segall *et al.*, 2001; Owen *et al.*, 2000b), the Long Valley-Inyo-Mono chain, California (Endo and Iwatsubo, 2000; Dixon *et al.*, 1997; Webb *et al.*, 1995), and several volcanoes in Japan. More are surely on the way. A preliminary instrument-siting plan for the Plate Boundary Observatory (PBO) in the western U.S.A. calls for clusters of 10–30 CGPS stations at several volcanoes in the Aleutian volcanic arc, Cascade Range, Long Valley-Inyo-Mono chain, and Yellowstone region (PBO Steering Committee, 1999). CGPS stations, borehole strainmeters and tiltmeters, improved interferometric synthetic-aperture radar (InSAR) coverage, and repeated geodetic surveys are essential components of a comprehensive volcano-monitoring program, which can be expected to yield fundamental new insights into how volcanoes operate (Dzurisin, 2003) (Chapter 11).

An excellent example of the utility of CGPS monitoring for revealing volcanic processes in unprecedented detail comes from Hawai'i, where Owen *et al.* (2000b) and Segall *et al.* (2001) analyzed CGPS data for the 30 January 1997 eruption at Napau Crater on the East Rift Zone of Kīlauea Volcano. The eruption occurred within a network of CGPS stations that recorded the temporal history of deformation during dike intrusion beginning ~8 hours prior to the onset of the eruption. Modeling results constrain the location, length, width, thickness, depth, strike, and dip of the dike. The authors concluded that: (1) magma was supplied to the eruption site from multiple sources, including the summit magma reservoir, a storage zone near Makaopuhi crater on the upper East Rift Zone, draining of the active lava pond at Pu'u 'Ō'ō, and perhaps elsewhere in the rift zone; (2) the intrusion was caused by continued deep rift zone inflation and slip on Kīlauea's south flank décollement, rather than by over-pressurization of stored magma; (3) the rate of dike propagation was limited by flow of magma into the dike; and (4) the volume of Kīlauea's summit magma reservoir is ~20 km^3, consistent with recent estimates from seismic tomography (Dawson *et al.*, 1999). Such far-ranging and detailed insights likely would not have occurred without the CGPS network data.

To have learned this much about the internal structure and dynamics of Kīlauea from a single, relatively small event is very impressive, indeed. Furthermore, these results hint at even greater discoveries to come as growing networks of CGPS stations, strainmeters, and tiltmeters continuously monitor Kīlauea's ever-changing shape, and as increasingly detailed models reveal new aspects of its structure. Kīlauea is not alone in this regard, as many of the world's prominent volcanoes (e.g., Krafla, Iceland; Long Valley-Inyo-Mono chain, U.S.A.; Mount Etna, Italy; Rabaul, Papua New Guinea; Piton de la Fournaise, Réunion Island, Indian Ocean; Sakurajima, Japan; Soufriere Hills, Montserrat, West Indies; Taal; Philippines; Yellowstone, U.S.A.) are being examined with CGPS and other modern geodetic tools.

3.5 SOME CAUTIONS ABOUT NEAR-SURFACE DEFORMATION SENSORS

No geodetic sensor, however sophisticated in design, can provide useful information about volcanic processes unless it is well coupled to a representative piece of the Earth and isolated from unmonitored environmental effects. That might seem like a simple matter, but in fact it is a notoriously difficult issue to address with any consistency. This is especially true when time is short, as during most volcano emergencies, or where the surface consists of deeply

weathered soil, fragmental debris, or intensely fractured rock, as is often the case near volcanoes. The most straightforward approach to mitigating this problem is to install all instruments in deep boreholes, far removed from insubstantial surface materials and capricious environmental effects. However, as emphasized by Agnew (1986, p. 596), '*The surface of the earth has two outstanding advantages as a place to put strainmeters and tiltmeters: it is accessible at low cost, and there is plenty of room.*' If for no other reason than this, surface installations will continue to dominate at most volcanoes for the foreseeable future.

One way to avoid the vagaries of near-surface installations is to take advantage of pre-existing tunnels, caves, or boreholes wherever possible. Agnew (1986) mentioned some advantages of this approach (e.g., reduced thermal effects), but also noted two disadvantages: (1) such openings may not be available where measurements are needed; and (2) instruments installed in such openings may not measure what is intended because the openings themselves distort the strain field. The ideal case, which can only be approximated in practice, is to bore a hole in competent bedrock well below the water table (preferably 100 m or more deep), case it with a watertight pipe, and couple a well-designed tiltmeter or strainmeter to the pipe.

Where such elaborate installations are not feasible (the general case), near-surface installations will suffice in most cases if simple precautions are observed to reduce temperature and precipitation effects. Burial of the sensor and any related electronics even by a few meters will help considerably, and usually can be accomplished in a single day's work. Attaching the sensor to several metal rods that have been driven to refusal in unconsolidated ground, coupled together, and partly encased in concrete is usually effort well spent. Finally, a sturdy housing to protect surface components of the installation (e.g., telemetry mast and antenna) from the worst of the elements is essential. Never underestimate the destructive power of nature (e.g., wind, heavy snow, or rime ice). Building a more robust monitoring station in good weather is always preferable to fixing a substandard one in a blizzard or rainstorm.

The following recommendations on the use of near-surface tiltmeters for volcano monitoring apply in part to other continuous sensors as well, and they still seem as pertinent as when they were first published (Dzurisin, 1992a). Out of necessity or oversight, I have violated these guidelines in the past and may do so again in the future. Nonetheless, to the extent possible:

(1) **Be skeptical**. Resist the temptation to interpret tiltmeter data until adequate baseline information is available for each station. Remember that substantial ground tilt can be caused by site responses to installation of the tiltmeter, freeze/thaw cycles, heavy rainfall, groundwater changes, and other factors unrelated to volcanic activity.
(2) **Never believe a single tiltmeter**. Design a tiltmeter network with enough redundancy to compensate for unreliable stations that are likely to exist, regardless of the amount of effort expended during installation.
(3) **Never believe a single dataset**. Interpret tiltmeter data only within the context of other monitoring information and in light of the recent eruptive history of the volcano.
(4) **Be conscious of the social and economic impact of your work**. Impacts can be either positive (e.g., reduction of damage to life or property) or negative (e.g., hardships caused by unnecessary evacuation or decrease in property values), but in either case they are likely to be substantial.

3.6 CONTINUOUS GRAVIMETERS

As discussed in the previous chapter, gravimeters are sensitive to two processes that commonly occur at active volcanoes: (1) changes in the height of the ground surface, and (2) changes in the subsurface distribution of mass. Therefore, repeated gravity measurements at a volcano are a useful tool for studying both surface deformation and subsurface changes in mass or density that might be caused by magmatic processes. There are two ways to obtain such measurements: (1) by repeatedly surveying a network of bench marks using a portable gravimeter; and (2) by installing one or more continuous gravimeters, which produce a continuous record of the local gravitational acceleration, g. Good spatial and temporal coverage can be obtained by combining both approaches. Such information is especially valuable if independent measurements of surface height changes (e.g., from leveling or GPS) and groundwater levels (e.g., from monitored wells) are available, so their effects can be removed from the gravity data.

Despite their potential for illuminating magmatic

processes, few continuous gravimeters have been operated on volcanoes for extended periods of time. This is mainly because the instruments are relatively expensive to install and maintain, and the data obtained reflect the combined effects of surface height changes, groundwater fluctuations, instrumental drift, and environmental factors. Without other, independently determined monitoring data, these factors are difficult to separate and remove from the gravity data. Nonetheless, continuous gravimeters are likely to see increasing use at volcanoes, as they become more affordable and as more volcanoes are monitored continuously for surface-height changes and groundwater fluctuations. For a more thorough discussion of gravitational principles, instruments, and techniques, the reader might want to consult an applied geophysics textbook, such as Chapter 2 in Telford *et al.* (1990).

3.6.1 Absolute gravimeters

Continuous gravimeters can be classified further as either absolute gravimeters or relative gravimeters. Both types can provide useful information at volcanoes. One type of absolute gravimeter, the free-fall gravimeter, makes straightforward and very precise measurements of the time t it takes an object to fall a distance d in a vacuum. The measurements are then fit to the appropriate equation of motion, $d = gt^2/2$, to determine the local value of g (Faller, 1967). Typical free-fall gravimeters consist of four main components: (1) an evacuated chamber with a freely falling test mass, (2) a reference test mass that is held in isolation from nongravitational accelerations and other background noise, (3) a laser interferometer, and (4) an atomic clock. Laser light is directed onto the test masses, and the reflected light is combined with the laser reference to produce interference fringes. The optical signal is sent to a photo detector where the precise trajectory of the falling mass is sampled, resulting in many time-and-distance pairs that are fit to the motion equation to determine an absolute value for g (Niebauer and others, 1986).

The precision and accuracy of free-fall gravimeters were estimated to be about 10 μGal until 1993, when a new generation of instrument called the FG5 became commercially available (Sasagawa *et al.*, 1995). The FG5 uses an iodine stabilized He–Ne laser and a rubidium atomic clock as length and time standards, respectively. It measures sets of time t and falling distance d of a free-falling corner cube in a vacuum chamber. The FG5's claim of 1–2 μGal accuracy and precision has been verified by intra-comparison of FG5 instruments (Sasagawa *et al.*, 1995; Niebauer *et al.*, 1995) and by comparison of the FG5 to a superconducting gravimeter (Okubo *et al.*, 1997; Francis *et al.*, 1998). The theoretical free-air gravity gradient is $-3.086\ \mu\text{Gal cm}^{-1}$ so this corresponds to 3–7 mm of height change in the absence of any mass change, which is adequate to detect vertical ground movements at many volcanoes.

Rise-and-fall absolute gravimeters are a more recent innovation that, as the name implies, make measurements during both the upward and downward parts of a free-fall trajectory. A test mass is thrown upward repeatedly in an evacuated chamber and its trajectory is tracked precisely using a laser interferometer and atomic clock (Brown *et al.*, 1999). Rise-and-fall gravimeters have several advantages over drop-only designs. The rise-and-fall symmetry results in cancellation of many classes of errors, including air resistance and magnetic field errors. Frequency dependent errors in the system electronics also are eliminated (Marson and Faller, 1986). Rise-and-fall gravimeters are substantially smaller and faster to use than their drop-only counterparts. A drop-only gravimeter spends a relatively large amount of time gently lifting the test mass, letting it settle at the top, and then waiting for it to gain an acceptable initial velocity to begin measurements. In contrast, rise-and-fall gravimeters accelerate the test mass upward very quickly, measure on both sides of the trajectory, and finish at the initial starting point. In one experiment with a rise-and-fall gravimeter, a throw rate of $1\ \text{s}^{-1}$ for 100 s resulted in a standard deviation in the measured value of g of ±1.5 μGal (Brown *et al.*, 1999).

3.6.2 Relative gravimeters – the magic of zero-length springs and superconductivity

Relative gravimeters measure differences in the acceleration due to gravity at different locations or times. In 1932, Lucien LaCoste, a graduate student at the University of Texas, and his faculty advisor, Dr. Arnold Romberg, developed a revolutionary design for portable instruments of this type. The elegance of the design, which still defines the state-of-the-art, merits a brief explanation. LaCoste and Romberg set out to develop a vertical long-period seismograph, akin to the horizontal pendulum seismograph used to record horizontal ground motions caused by earthquakes. In a horizontal

pendulum seismograph, a mass attached to one end of a rigid beam is free to oscillate in a horizontal plane about a vertical hinge near the other end of the beam. If the axis of the hinge is perfectly vertical, the mass and beam form a horizontal pendulum with an infinite period. Any slight departure from verticality allows gravity to act as a damping force, decreasing the period of the pendulum and thus its sensitivity to horizontal accelerations.

LaCoste and Romberg wondered if a similar device could be constructed to measure vertical motions. This would require a mechanism to precisely counterbalance the force of gravity, so a mass attached to a beam with a horizontal hinge could be 'suspended' and allowed to oscillate in a vertical plane. A sketch of the required suspension is shown in Figure 3.12. The goal is to use a spring to precisely counterbalance the gravitational torque on a mass at the end of a beam. The gravitational torque is:

$$T_g = Wd \sin \theta \tag{3.1}$$

where W is the weight of the mass, $W = mg$, and d is the distance from the center of the mass to the beam's hinge. The torque due to the spring is the product of the force exerted by the spring and the spring's lever arm, and can be written as (LaCoste and Romberg, 1998; Bomford, 1980, pp. 375–377):

$$T_s = -k \times (l - l_0) \times s = kl_0 s - k \times \frac{b \sin \theta}{\sin \beta} \times a \sin \beta$$
$$= kl_0 s - kab \sin \theta \tag{3.2}$$

where s is the lever arm, k is the spring constant, l and l_0 are the lengths of the stretched and unstretched spring, respectively, and a, b, α, β, and θ are the distances and angles shown in Figure 3.12. The total torque on the mass is:

$$T = T_g + T_s = Wd \sin \theta + kl_0 s - kab \sin \theta$$
$$= kl_0 s + (Wd - kab) \times \sin \theta \tag{3.3}$$

Equating the total torque to zero, we obtain:

$$kl_0 s + (Wd - kab) \times \sin \theta = 0 \tag{3.4}$$

The second term can be engineered to equal zero by selecting an appropriate mass and spring constant, then arranging the geometry correctly. On the other hand, eliminating the first term is more challenging. The spring constant k, and the spring's lever arm s, have finite values, so the only option available to LaCoste and Romberg was to design a 'zero-length' spring (i.e., a spring with $l_0 = 0$). At first glance, this seems impossible. How can we design a spring that shrinks to zero length when no force is applied to it? LaCoste and Romberg realized they didn't have to. The trick is to engineer a spring that exerts an appropriate, non-zero force when the spring contracts to the point at which its coils touch one another. For such a spring, a plot of F versus l follows the relation $F = kl$, which passes through the origin when *extrapolated* to $l = 0$ (Figure 3.13). There are several ways to make a spring of this type. Modern LaCoste & Romberg gravimeters actually use a 'negative-length' spring in combination with fine wires to achieve the same effect (LaCoste and Romberg, 1998).

Modern LaCoste & Romberg gravimeters use this suspension together with a fine micrometer to adjust the extension of the spring and thus to counterbalance the gravitational torque to a precision of 1 μGal or less (Figure 3.14). The accuracy of properly corrected measurements made with such a meter in survey mode is typically about 5 μGal. For me, the graceful swings of the crosshair about the reading line when a LaCoste & Romberg gravimeter is perfectly adjusted in the local gravity field, especially at a bench mark within sight of an active volcano, elicit a feeling that borders on reverence. Such delicate mechanical balance provides a soothing counterpoint to the potential for volcanic mayhem.

In 2001, LaCoste & Romberg and Scintrex Ltd., merged to form a new company known as LaCoste & Romberg–Scintrex, Inc., which produces over 90% of the world's gravimeters. In 1989, Scintrex Ltd., developed a fused-quartz-based relative gravimeter, the CG-3, based on the Ph.D. thesis of another enterprising graduate student, Dr. Andrew Hugill. Today, the Scintrex CG-5 Autograv gravimeter, together with the LaCoste & Romberg Model G, Model D, and Graviton EG gravimeters, set the standards for precision and repeatability among portable gravimeters. Features include automatic noise rejection, self leveling and automatic tilt compensation, and automatic reading and internal data logging options.

Although portability is an important feature of zero-length-spring and fused quartz-sensor gravimeters, which are commonly used in survey mode to measure a network of gravity stations, an instrument of this type can also be operated at a single site for an extended period of time to produce a continuous record. The instrumental sensitivity is more than adequate to measure solid Earth tides, which can be removed from the record if desired to reveal residual signals caused by volcanic or tectonic processes, or by groundwater fluctuations. Unfortu-

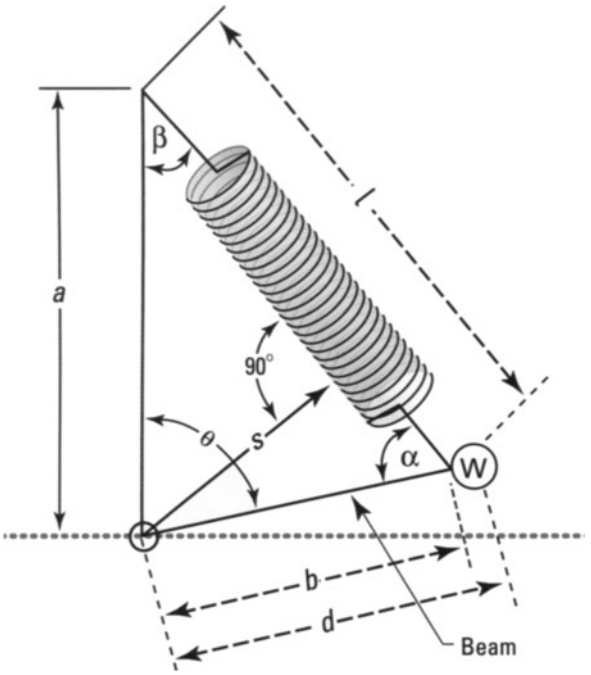

Figure 3.12. A suspension system for precisely counterbalancing the gravitational torque on a mass attached to a beam using a 'zero-length' spring (LaCoste and Romberg, 1998) (Figure 3.13). This ingenious mechanism is an essential component of LaCoste and Romberg gravimeters (Figure 3.14), which are suitable for volcano studies. See text, Section 3.6.2, for explanation of symbols.

nately, slow mechanical aging of the spring or other factors produce long-term drift that can be difficult to distinguish from other effects, including vertical surface movements and subsurface mass or density changes. Replacing the spring would only start the process over again. For applications where slowly varying, long-term signals might be important, as is the case for many volcanoes, other types of continuous gravimeters are a better choice.

One such design is the superconducting relative gravimeter, which balances the weight of a superconducting niobium sphere using a force produced by electrical current in a superconducting coil. Changes in the current needed to maintain the sphere at a null position are proportional to changes in the local gravity field (Francis *et al.*, 1998). These instruments sample the gravity field every 1–10 s with a precision of <1 nGal (10^{-9} Gal) and an estimated accuracy on the order of 0.1 μGal. Because electrical losses in a superconducting material are virtually zero, this design can achieve extremely low long-term drift rates, on the order of 1 μGal yr^{-1} (Crossley *et al.*, 1999). The best gravity-monitoring site would combine a superconducting relative gravimeter with co-located measurements by an absolute gravimeter at regular intervals, a strategy that has been implemented at Mount Vesuvius, Italy (see below).

3.6.3 Gravity results from selected volcanoes

A recording LaCoste & Romberg Model D gravimeter was installed at Mount Vesuvius in 1988. The instrument is located at the Osservatorio Vesuviano on a concrete pillar in a 20 m deep artificial cave, where the daily temperature excursion is about 0.1°C and the annual excursion is about 2°C. The station also is equipped with temperature, pressure, and tilt sensors. High-precision absolute gravity measurements were made at a nearby site in 1986, 1994, and 1996. The absolute gravity decreased by about 60 μGal from 1986 to 1994, then changed very little from 1994 to 1996 (Berrino *et al.*, 1997). EDM measurements of a 21-station, 60-line

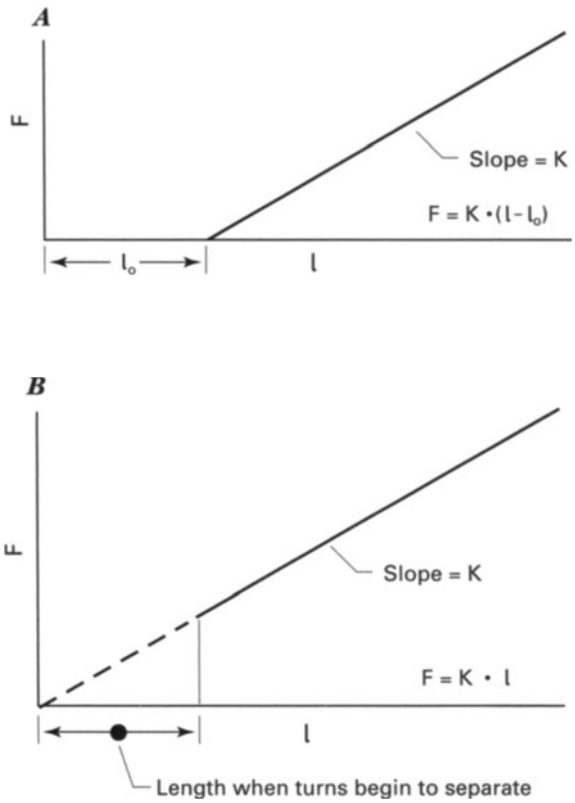

Figure 3.13. Relationship between force exerted by an ideal spring F and its length l. (A) For a typical spring, F is a linear function of l, and F approaches 0 as l approaches l_0, the unstretched length of the spring. (B) A 'zero-length' spring is designed such that it exerts a finite force $F = kl_0$ at its minimum length (when its coils touch each other) and such that F approaches 0 as l is extrapolated to 0 (LaCoste and Romberg, 1998).

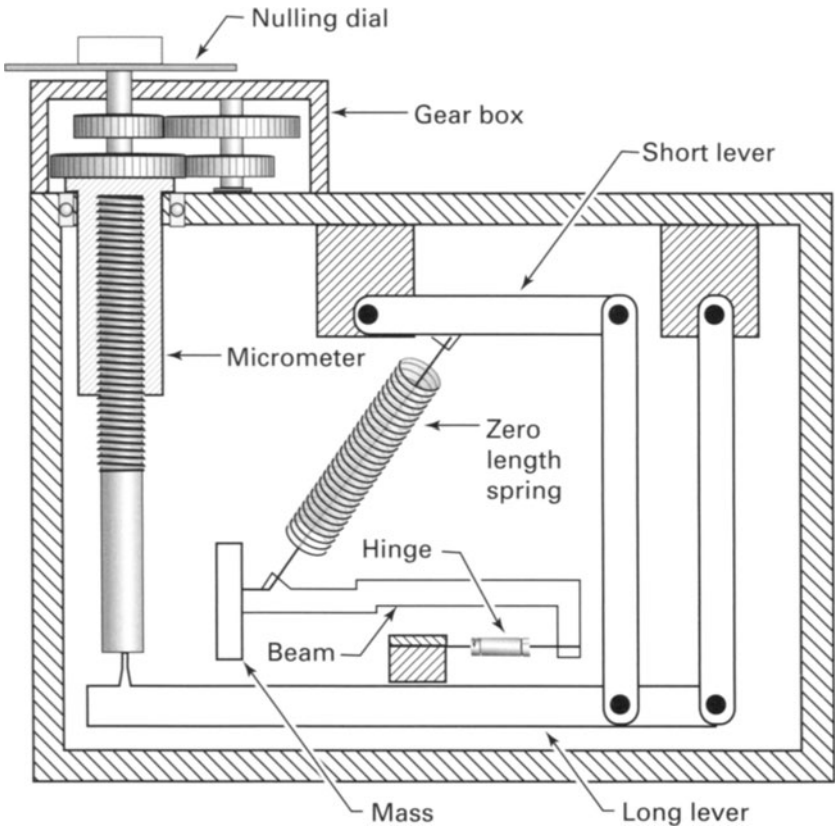

Figure 3.14. Schematic diagram showing the principal components of a LaCoste & Romberg gravimeter (LaCoste and Romberg, 1998).

trilateration network on the volcano revealed no significant ground deformation from 1975 to 1995 (Pingue *et al.*, 1998), which suggests that the observed gravity change was not caused by uplift. An analysis of the continuous gravity record revealed that the tidal amplification factor, which measures local gravitational response to solid Earth tides, increased by several per cent from 1988–1991 to 1994–1996. Berrino *et al.* (1997) suggested that both changes could have been caused by mass redistribution at depth (presumably withdrawal of material from beneath the gravity station with no associated surface deformation) or, alternatively, the increased amplification factor might indicate reduced crustal rigidity. Neither of the changes seemed to correspond with the intensity of local earthquake activity, which mostly fluctuated between about 10 and 100 earthquakes per month.

At Merapi Volcano, Indonesia, a recording gravimeter in the Babadan observatory has recorded long-term signals that correlate with seismic and volcanic activity (Jousset *et al.*, 2000). For example, the residual drift of the meter decreased steadily from November 1993 (when it was installed) to March 1994, then increased steadily until June 1994 when it stabilized. The trend reversal corresponded to a period of intense low-frequency earthquakes and nuées ardentes (i.e., dome-collapse pyroclastic flows) during March–April 1994. In addition, the gravimeter's admittance, a combination of the instrument's sensitivity (which is tilt dependent) and the mechanical response of the ground to tidal forces, decreased suddenly by almost 20% during the third week of April 1994, when a new phase of rapid dome extrusion began. Jousset *et al.* (2000) proposed a model in which extrusive activity was driven partly by internal pressure oscillations due to crystallization and degassing of magma in a shallow reservoir.

Continuous gravity results at Mount Etna, Sicily, are likewise intriguing (De Meyer *et al.*, 1995), although their interpretation is made difficult by the inability to sort out effects of ground deformation, magma movement or density changes, and groundwater fluctuations.

Taking full advantage of the potential of continuous gravimetry requires a substantial investment of funds, time, and effort. This is especially true be-

cause vertical surface displacements, groundwater fluctuations, and environmental changes also must be monitored continuously to remove their effects from the gravity signal. These difficulties aside, I believe this approach holds considerable promise for a significant advance in our understanding of volcanic processes, especially during non-eruptive periods when magmatic activity is hidden from direct observation.

3.7 DIFFERENTIAL LAKE GAUGING

Water-filled lakes are common features at volcanoes, and in some cases they provide a useful means to monitor ground deformation or surface volume changes related to eruptive activity. A lake on the flank of a volcano or near its base, for example, would exhibit differential water-level changes if the lakeshore tilted while the water surface remained horizontal. A crater lake at the summit of a volcano might not exhibit any differential tilt, but extrusion of a lava flow or dome onto the lake floor would raise the water level, while collapse of the floor would lower it. Both types of changes can be monitored by repeated surveys or continuously recording instruments.

If conditions are right, lake gauging can be a very useful volcano-monitoring technique. For example, periodic monitoring of water levels in a well-situated, 2 km diameter lake with an accuracy of ±2 mm could provide information about cross-lake tilt to an accuracy of ±1 μrad without having to deploy or maintain tiltmeters or other types of sensors. Alternatively, pressure transducers could be deployed in a lake to continuously sense water depth at several sites, thereby accumulating enough information to distinguish among the effects of wave action, seiche, filling and draining of the lake, and tilting of the lake basin. In practice, it is usually difficult to find a well-situated lake of sufficient size that does not freeze over in the winter and is not subject to violent wave action that can damage sensors. Nonetheless, if a suitable lake exists, consideration should be given to making use of it as a natural tiltmeter.

3.7.1 Monitoring active deformation at Lake Taupo, New Zealand

Lake Taupo occupies most of the 35 km diameter Taupo Caldera, which formed by collapse during eruption of the Taupo Pumice (90+ km^3 bulk volume) in 186 CE (Wilson *et al.*, 1984). Deformation of the area has been monitored since 1979 with a portable water-level gauge at sites around the shoreline and on two small islands (Otway and Sherburn, 1994). The standard deviation σ of lake-level measurements using this technique, based on the repeatability observed over short time periods, is $\pm[1.2 + (d \times 10^{-7})]$ mm, where d is the straight-line distance in kilometers between a reference site and some other measurement site. In the worst case (i.e., at the most distant site), $d \approx 40$ km and $\sigma \approx 5.2$ mm, which corresponds to a uniform tilt across the long axis of the lake of approximately 0.1 μrad.

From 1985 to 1990, vertical deformation measured with a portable water-level gauge at Lake Taupo and shallow seismicity there displayed two distinct patterns (Otway and Sherburn, 1994). In the Taupo Fault Belt north of the lake, subsidence at a maximum rate of 10 ± 1 mm yr^{-1}, which corresponds to inward tilt of more than 1.0 ± 0.1 μrad yr^{-1}, occurred steadily and nearly aseismically (Figure 3.15). In contrast, the central and southern parts of the lake tilted much more slowly to the southwest, but produced repeated small oscillations in height and frequent earthquake swarms. Short-term increases in the deformation rate preceded or accompanied four of the strongest swarms, but there was no apparent correlation between short-term deformation and individual seismic events.

Otway and Sherburn (1994) hypothesized that both patterns reflect responses, at different timescales and depths, to underlying strain release. They noted that extension rates across the southern Taupo Fault Belt north of Lake Taupo averaged 18 ± 5 mm yr^{-1} for the 30-year period before 1986 (Darby and Williams, 1991), so aseismic sag in that area might indicate crustal thinning resulting from back-arc spreading accompanying subduction. Farther south, the deformation and seismicity patterns suggest a distinctive style of strain release, although the reason for the difference is not known.

3.7.2 Lake terraces as paleo-tiltmeters

Lake terraces, like bathtub rings, form horizontally at the margin of a body of water and, therefore, indicate a surface that was initially level. Any subsequent deformation of the lake margin is recorded by terraces as a departure from horizontality, which can be measured by surveying. Typically, terraces are not continuous along an entire lake margin, both

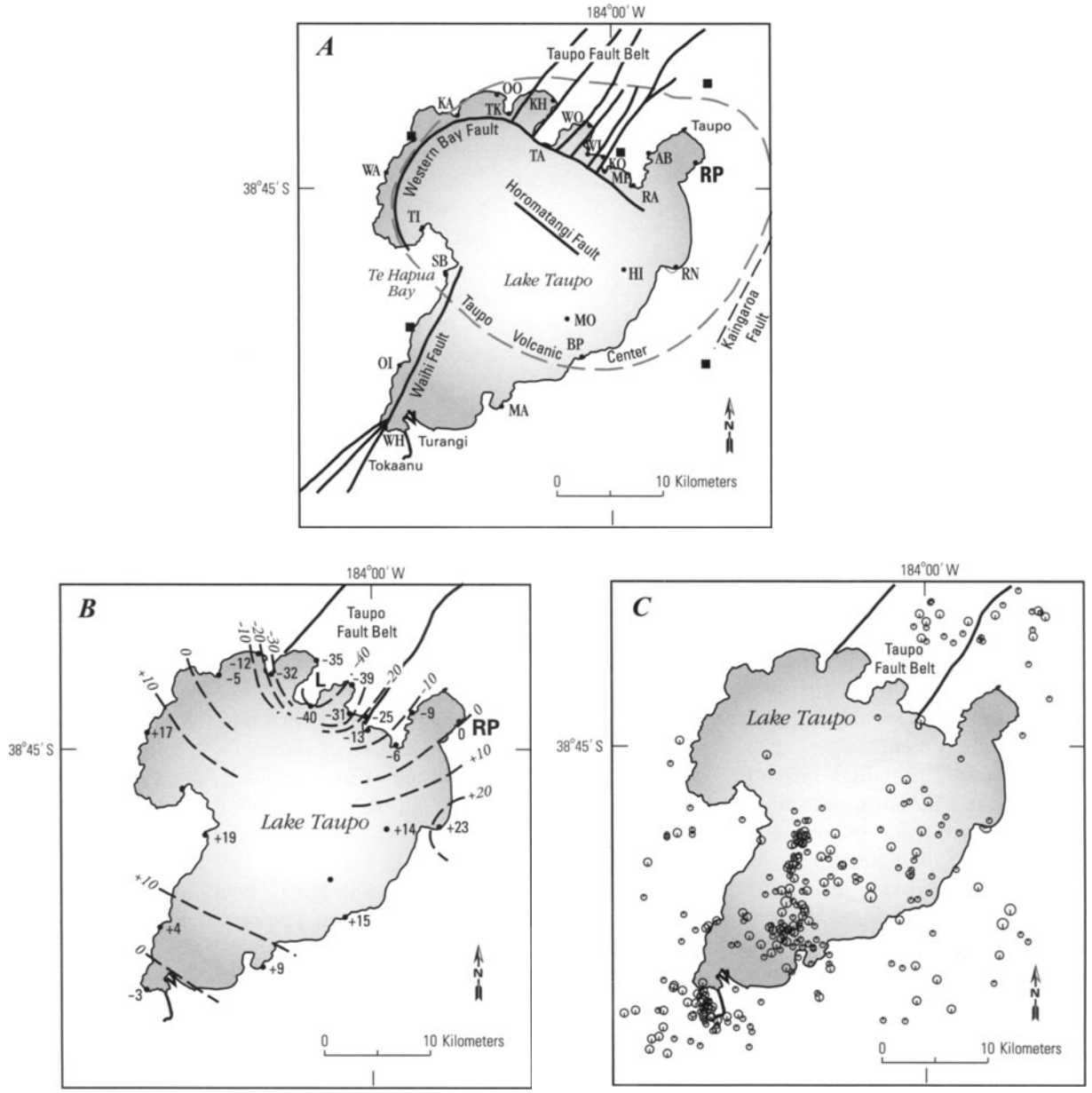

Figure 3.15. Deformation and seismicity near Lake Taupo, New Zealand, 1985–1990 (Otway and Sherburn, 1994). (A) Locations of lake leveling sites (dots), seismographs (squares), and main faults. (B) cumulative shoreline height changes, in mm relative to reference station RP, between 10 December 1985 and 6 December 1990, from repeated lake leveling surveys. Standard deviations are 3–7 mm and increase with distance from RP. (C) Epicenters of earthquakes of $M_L \geq 2.6$ (local magnitude, see Glossary entry 'earthquake magnitude' at the back of this book) between September 1985 and December 1990. Symbol size varies with earthquake magnitude.

because they do not form everywhere and because subsequent lake-level changes and wave action tend to remove terrace segments. Nonetheless, in some cases a deformation history can be pieced together through careful mapping, correlation, dating, and surveying of remnant terrace surfaces. Two such cases are Yellowstone Lake, Wyoming, which straddles the southeast rim of Yellowstone Caldera, and Paulina Lake, Oregon, one of two lakes that occupy the summit caldera of Newberry volcano.

The shorelines of Yellowstone Lake record a rich Holocene deformation history, including two major cycles of uplift and subsidence that were each thousands of years long and tens of meters in amplitude

(Pierce *et al.*, 2002; Locke and Meyer, 1994; Hamilton and Bailey, 1988; Bailey and Hamilton, 1988; Meyer and Locke, 1986). Cyclic tilting of the lake basin alternately raised and lowered the lake outlet, causing high and low stands of the lake, respectively. The resulting shoreline terraces range from about 30 m below the present shoreline to about 20 m above it. Over the entire postglacial period (15,000 years), subsidence has balanced or slightly exceeded uplift, as shown by older shorelines that *descend* toward the caldera axis. These millennia-scale deformation cycles are akin to decadal-scale ups and downs of the caldera floor that have been revealed by repeated leveling, GPS, and InSAR observations (Dzurisin *et al.*, 1990, 1994, 1999; Wicks *et al.*, 1998) (Chapter 7).

Several processes might contribute to deformation at Yellowstone at different times and to varying degrees. These include magma intrusion or withdrawal, cooling of magma or hot rock, tectonic extension, and fluid pressure changes driven by magmatic volatiles and modulated by episodic cracking of a self-sealed layer in the deep hydrothermal system (Fournier, 1999; Dzurisin *et al.*, 1990). The hydrothermal mechanism is favored for both the historical and Holocene time periods, because it provides for both uplift and subsidence with little overall change (Pierce *et al.*, 2002; Dzurisin *et al.*, 1990).

At Newberry volcano in central Oregon, deformed lakeshore terraces and a nearby outlet stream preserve evidence for a large flood and subsequent uplift within the summit caldera. Newberry's 6×7 km caldera contains two lakes, Paulina Lake and East Lake, and has been the site of several eruptions during the past 10,000 years (MacLeod *et al.*, 1995). Along the channel of Paulina Creek, which drains Paulina Lake, a flood about 1,800 years ago swept away the regional Mazama Ash, deposited coarse gravel, eroded bedrock channels, and dropped lake level by as much as 1.5 m. Shoreline terraces that were abandoned when lake level dropped were subsequently tilted and displaced vertically upward by as much as 4–6 m (Jensen and Chitwood, 1996). It remains to be seen whether the flood or caldera deformation can be related to eruptions that produced rhyolitic pumice-fall deposits about 1,600 years ago or Big Obsidian Flow and associated ashflow deposits about 1,300 years ago (MacLeod *et al.*, 1995).

3.8 CONCLUDING REMARKS

This chapter has touched upon a wide variety of *in situ* sensors and techniques that volcanologists can draw upon to monitor deforming volcanoes. The best choices for a particular situation depend upon such things as the nature of the mission (hazards mitigation, curiosity driven research, or both), risk level (people, property, and major infrastructure), type of volcano (frequently active or long dormant, dominantly explosive or effusive), logistics (ease of access, year-round maintenance requirements), and available resources. No single type of sensor or combination of sensor types is appropriate for all situations, nor is a cookie-cutter approach to deformation monitoring likely to be successful. A monitoring program tailored to a specific set of circumstances and based on flexibility and innovation is usually the best alternative.

The GPS is likely to be a key component of any such program, for several reasons. GPS is flexible, precise, easy to use, universally accessible, and generally affordable. In the following chapter I examine this modern marvel and a few of its many applications to geodesy and volcano monitoring.